

國立交通大學

電信工程學系碩士班
碩士論文

適用於移動式 WiMAX 系統之疊代式通道估
計與載波間干擾消除技術

Iterative Channel Estimation and ICI Cancellation
for Mobile WiMAX Systems

研究生：蔡嘉航

Student: Chia-Hang Tsai

指導教授：李大嵩 博士

Advisor: Dr. Ta-Sung Lee

中華民國九十六年六月

適用於移動式 WiMAX 系統之疊代式通道估計與載波
間干擾消除技術

Iterative Channel Estimation and ICI Cancellation for
Mobile WiMAX Systems

研究生：蔡嘉航

Student: Chia-Hang Tsai

指導教授：李大嵩 博士

Advisor: Dr. Ta-Sung Lee



A Thesis

Submitted to Institute of Communication Engineering
College of Electrical Engineering and Computer Science

National Chiao Tung University

in Partial Fulfillment of the Requirements

for the Degree of

Master of Science

in

Communication Engineering

June 2007

Hsinchu, Taiwan, Republic of China

中華民國九十六年六月

適用於移動式 WiMAX 系統之疊代式通道估計 與載波間干擾消除技術

學生：蔡嘉航

指導教授：李大嵩 博士

國立交通大學電信工程學系碩士班

摘要

正交分頻多工系統為新一代無線通訊系統最常使用的技術，如 IEEE 802.11a/g/n、IEEE 802.16、IEEE 802.20、數位電視、數位廣播等許多系統均採用此技術。傳統的正交分頻多工系統並不適用在高速移動的環境中，然而移動傳輸是未來無線通訊系統的趨勢之一，如 IEEE 802.16-2005 可支援到車速 120 km/hour，而 IEEE 802.20 更可支援到車速 250 km/hour。傳統的正交分頻多工系統可以有效率地使用在非時變通道中，且僅需簡單的等化器，即可修正通道效應，但在移動的環境中，通道隨著時間改變，使得接收端的子載波失去正交性，因而導致子載波之間的相互干擾，使得解調變後的效能降低。在本論文中，吾人設計出一個疊代式通道估計與載波間干擾消除技術，其利用通道估計結果將 ICI 以數學模型趨近表示之，使接收端得以有效併行地消去子載波間的干擾，而能在移動的環境下運作。吾人藉由電腦模擬驗證此一新演算法在移動的環境中並使用 IEEE 802.16-2005 的規格下，可有效改善位元錯誤率。

Iterative Channel Estimation and ICI Cancellation for Mobile WiMAX Systems

Student: Chia-Hang Tsai

Advisor: Dr. Ta-Sung Lee

Department of Communication Engineering
National Chiao Tung University

Abstract

Orthogonal Frequency Division Multiplexing (OFDM) is a popular technique in modern wireless communications. There are many systems adopting the OFDM technique, such as IEEE 802.11 a/g/n, IEEE 802.16, Digital Video Broadcasting, etc. On the other hand, mobile transmission is a trend in future wireless communications. For example, IEEE 802.16-2005 supports vehicle speed up to 120 km/hour. OFDM systems can be used efficiently in time invariant environments with one-tap equalizers. However, subcarriers are no longer orthogonal to each other in time-varying channels, and this causes the intercarrier interference (ICI) and degrades the system performance. To alleviate this problem, we propose an iterative ICI mitigation and time-varying channel estimation scheme, which can obtain the ICI information from the channel estimate using piece-wise linear or Taylor series approximate and then cancel it in parallel fashion. The proposed PIC structure and the overall iterative system structure designed are discussed in detail. Finally, we evaluate the performance of the proposed system under mobility using IEEE 802.16-2005 standard and confirm that it achieves good BER performance.

Acknowledgement

I would like to express my deepest gratitude to my advisor, Dr. Ta-Sung Lee, for his enthusiastic guidance and great patience. I also wish to thank my friends for their encouragement and help. Finally, I would like to show my sincere thanks to my parents for their inspiration and love.



Contents

Chinese Abstract	I
English Abstract	II
Acknowledgement	III
Contents	IV
List of Figures	VII
List of Tables	IX
Acronym Glossary	X
Notations	XII
Chapter 1 Introduction.....	1
Chapter 2 Overview of Mobile WiMAX System	4
2.1 Physical Layer Description.....	5
2.1.1 Randomizer	6
2.1.2 Forward Error Correction	7
2.1.3 Interleaver	9
2.1.4 Modulator.....	9



2.1.4.1	Pilot Modulation	9
2.1.4.2	Preamble Structure	10
2.2	Key Features of Scalable OFDMA	11
2.2.1	Scalable Channel Bandwidth	11
2.2.2	Sub-channelization and Permutation	12
2.2.3	Fractional Frequency Reuse.....	17
2.3	Transmit Techniques	18
2.3.1	Transmit Diversity: Space-Time Coding	19
2.3.2	Transmit Beamforming: Adaptive Antenna System	22
2.4	Summary	24
Chapter 3 Channel Estimation for Mobile WiMAX System ..		26
3.1	Channel Model.....	27
3.1.1	SUI Channel Model for Fixed Wireless Application	27
3.1.2	ITU Channel Model for Mobile Wireless Application	32
3.1.3	SCM Channel Model for Mobile MIMO Wireless Application	34
3.2	Channel Estimation.....	36
3.2.1	LS and MMSE Channel Estimation.....	39
3.2.2	Interpolation Techniques.....	41
3.2.3	Time Domain LS Channel Estimation.....	42
3.3	Summary	46
Chapter 4 ICI Mitigation for Mobile WiMAX Systems.....		47
4.1	Channel Analysis with ICI Induced by Mobility	48

4.2	ICI Modeling.....	51
4.2.1	Piece-wise Linear Model	51
4.2.2	Taylor Series Modeling.....	55
4.3	Combined Channel Estimation and ICI Mitigation	59
4.3.1	Data Detection Techniques	59
4.3.2	PIC Equalizer	60
4.3.3	Complexity Issue	63
4.4	Computer Simulations	64
4.5	Summary	72
Chapter 5 Conclusion.....		73
Bibliography		75



List of Figures

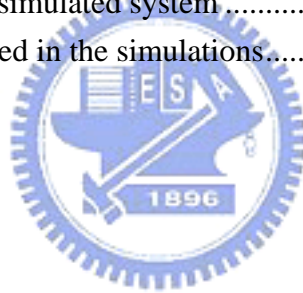
Figure 2-1	PRBS generator for randomizer	6
Figure 2-2	OFDMA randomizer DL initialization vector	7
Figure 2-3	Convolutional encoder	8
Figure 2-4	PRBS generator for pilot modulation.....	10
Figure 2-5	Example of DL preamble for segment 1	11
Figure 2-6	Cluster structure	13
Figure 2-7	Allocated subcarriers into subchannels for PUSC	14
Figure 2-8	Example of mapping OFDMA slots to subchannels and symbols in DL PUSC	15
Figure 2-9	Description of a UL PUSC tile.....	15
Figure 2-10	Allocated subcarriers into subchannels for FUSC	16
Figure 2-11	AMC bin structure.....	17
Figure 2-12	Description of fractional frequency reuse	18
Figure 2-13	Block diagram of STC.....	20
Figure 2-14	Illustration of Alamouti scheme	20
Figure 2-15	Cluster structure for STC PUSC using 2 Antennas.....	22
Figure 2-16	Illustration of AAS	23
Figure 2-17	Generalized AAS zone allocation.....	24
Figure 2-18	AAS zone structure in OFDMA mode	24
Figure 3-1	Doppler spectrum of SUI channel models	30
Figure 3-2	Doppler spectrum of ITU channel models	34
Figure 3-3	BS and MS angular parameters in SCM specification.....	35
Figure 3-4	Baseband model of a typical pilot-based system	36
Figure 3-5	Pilot-aided channel estimation scheme	41
Figure 3-6	Comparison with two channel estimation methods.....	46
Figure 4-1	Plot of channel matrix	50
Figure 4-2	Piece-wise linear model	52
Figure 4-3	Piece-wise linear model using symbols nearby.....	52
Figure 4-4	Mean square error of different approximations to the varying channel	

	58
Figure 4-5	Magnitude of different approximations to the varying channel	58
Figure 4-6	Nearest point data detection method	60
Figure 4-7	PIC structure.....	61
Figure 4-8	System Structure.....	63
Figure 4-9	Comparison of schemes without and with ICI compensation in second-order varying channel	67
Figure 4-10	Comparison with different blocks with different SNR.....	68
Figure 4-11	Comparison with different blocks with different velocity.....	68
Figure 4-12	BER performance of different d in 150 km/hr	69
Figure 4-13	BER performance for different modulation schemes in 120 km/hr	70
Figure 4-14	BER performance for different methods of 512-FFT in 100 km/hr.....	71
Figure 4-15	BER performance for different methods of 512-FFT in high SNR.....	71



List of Tables

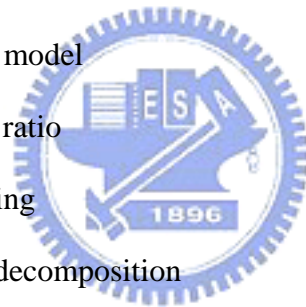
Table 2-1	Data rate for different modulations and code rates	5
Table 2-2	Puncturing patterns and orders to realize different code rates	8
Table 2-3	Useful data payload for a slot.....	8
Table 2-4	OFDMA scalability parameters for different bandwidth	12
Table 3-1	Parameters of SUI-3 channel models	28
Table 3-2	Parameters of ITU channel models	33
Table 4-1	Iterative ICI cancellation procedure.....	63
Table 4-2	parameters of the simulated system	65
Table 4-3	Channel model used in the simulations.....	66



Acronym Glossary

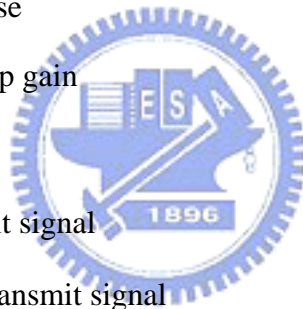
3GPP	third generation partnership project
AAS	Adaptive Antenna System
AMC	Adaptive Modulation and Coding
AOA	angle of reception
AOD	angle of departure
AWGN	additive white Gaussian noise
BS	base station
CCIR	co-channel interference rejection
CINR	carrier-to-interference-and-noise ratio
DL	downlink
DFT	discrete fourier transform
FFT	fast fourier transform
FUSC	Full Usage of Subchannels
IEEE	institute of electrical and electronics engineers
ICI	inter-carrier interference
IDFT	inverse discrete fourier transform
IFFT	inverse fast fourier transform
ISI	inter-symbol interference
ITU	international telecommunication union
LOS	line-of-sight

LS	least square
MMSE	minimum mean square error
MS	mobile station
NLOS	non-line-of-sight
OFDM	orthogonal frequency division multiplexing
OFDMA	orthogonal frequency division multiple access
PIC	parallel interference cancellation
PUSC	Partial Usage of Subchannels
QAM	quadrature amplitude modulation
QOS	quality of service
QPSK	quadrature phase shift keying
SCM	spatial channel model
SNR	signal-to-noise ratio
STC	space time coding
SVD	singular value decomposition
UL	uplink
WiMAX	worldwide interoperability for microwave access



Notations

BW	bandwidth
N	FFT size
L	maximum length of the channel
G	maximum delay of the channel
H	channel frequency response
h	channel time response
g	multipath channel tap gain
τ	multipath delay
x	time domain transmit signal
X	frequency domain transmit signal
y	time domain receive signal
Y	frequency domain receive signal
P	pilot magnitude
f	pilot subcarrier index
d	number of neighboring points to generate the ICI estimate
q	number of subcarriers used for data transmission
w	time domain AWGN noise
W	frequency domain AWGN noise
T_s	sampling time



Chapter 1

Introduction

Wireless communication systems have been in use for quite a long time. Many standards are available based on which user devices communicate, but the present standards fail to provide sufficient data rate, when the user is moving at high speed. Broadband wireless access is an appealing way to provide flexible and easily-to-deploy solution for high speed communications. In view of this requirement for future mobile wireless communication systems, the 802.16 standard has been proposed by Institute of Electrical and Electronic Engineers (IEEE) [1], [2].

The WiMAX (Worldwide Interoperability for Microwave Access) Forum is committed to providing optimized solutions for fixed, nomadic, portable and mobile broadband wireless access. Two versions of WiMAX address the demand for these different types of access:

- **IEEE 802.16-2004:** This is based on the 802.16-2004 version of the IEEE 802.16 standard. It uses Orthogonal Frequency Division Multiplexing (OFDM) and supports fixed and nomadic access in Line of Sight (LOS) and Non Line of Sight (NLOS) environments. For LOS environment, the frequency range in 802.16d is from 2GHz to 66GHz and Single Carrier (SC) is mainly adopted as the transmission scheme. For NLOS environment, it focuses on the Broadband Wireless Access (BWA), where the frequency band ranges from 2GHz to 10GHz. In physical layer (PHY),

NLOS temps to adopt OFDM and OFDMA techniques.

- **IEEE 802.16-2005:** Optimized for dynamic mobile radio channels. This version is based on the IEEE 802.16-2005 amendment and provides support for handoffs and roaming. The choice of the subcarrier number becomes more flexible since it provides four options, 128, 512, 1024, and 2048, in contrast to the single choice of 2048 in IEEE 802.16-2004. The frequency band ranges from 2GHz to 6GHz.

Orthogonal Frequency Division Multiplexing (OFDM) is a popular technique in modern wireless communication systems. In an OFDM system, the bandwidth is divided into several orthogonal subchannels for transmission. A cyclic prefix (CP) is inserted before each symbol. Therefore, if the delay spread of the channel is shorter than the length of the cyclic prefix, the intercarrier symbol interference (ISI) can be eliminated due to the cyclic prefix. On the other hand, subcarriers in OFDM are orthogonal to each other over time-invariant channels, so the conventional OFDM system only requires one-tap equalizers [3] to compensate the channel response. This characteristic simplifies the design of the OFDM receiver, and for this reason, the OFDM technique is widely used in wireless communication systems.

The mobile transmission is a trend in future wireless communications. Many systems support the mobile transmission. However, while OFDM system is applied in mobile environments, the reliability of OFDM is limited because of the time-varying nature of the channel. This leads to the loss of subcarrier orthogonality, which, in turn, yields intercarrier interference (ICI) and increases inaccuracies in channel tracking. The effect of channel variations for the ICI has been addressed in [4]. Therefore, the ICI cancellation technique plays an important role in mobile OFDM systems.

Although the problem of robust OFDM reception in mobile environment and solutions for ICI mitigation have been addressed recently by several researchers, they

are not practical due to the complexity of reducing the ICI effect and the incompatibility with the 802.16 standards. For example, the precoding solution for self-cancellation [5] requires a modification of the transmit format such that it is incompatible with the existing transmit schemes. If ICI is modeled as an additional Gaussian random process [4] and not adequately compensated, the ICI will result in a severe error floor. Robust channel estimation using time and frequency domain correlation with H_∞ approach [6] results in a large computation delay in adopting the singular value decomposition (SVD) and the H_∞ estimation algorithms. The ML iterative estimator [7] and adaptive matrix equalizer [8] require a large computation load and thus lose their feasibility at high speeds or become too complex for commercial products. In this thesis, an iterative ICI mitigation and time-varying channel estimation scheme are proposed to solve the problem, which include the time domain channel estimator, ICI modeling using derivatives of the channel variation based on [7], [9], and the parallel interference cancellation (PIC) equalizer similar to [10], which consists of a set of one-tap equalizers and a set of ICI cancellation filters to both compensate for the multiplicative distortion and cancel the ICI.

The rest of this thesis is organized as follows. In Chapter 2, an overview of WiMAX system is given. The transmit techniques such as Space-Time Coding (STC) and Adaptive Antenna System (AAS) are also introduced. In Chapter 3, channel models being used are introduced and several channel estimation approaches that fit the IEEE 802.16 standard are discussed. In Chapter 4, we propose a PIC equalizer to suppress the channel effect in mobile concern, several computer simulation results are also given to show the performance improvement of the proposed ICI cancellation system structure in IEEE 802.16-2005 system. In Chapter 5, we conclude this thesis.

Chapter 2

Overview of Mobile WiMAX System

WiMAX is a broadband wireless technology that supports fixed, nomadic, portable and mobile access. To meet the requirements of different types of access, two versions of WiMAX have been defined. The first is based on IEEE 802.16-2004 and is optimized for fixed and nomadic access. The second version is designed to support portability and mobility, and will be based on the IEEE 802.16-2005 amendment to the standard. In this chapter, we will focus on the physical layer of orthogonal frequency division multiple access (OFDMA) structure in IEEE 802.16-2005 and provide a detail introduction of Scalable OFDMA (SOFDMA) technology. Finally, the transmit techniques such as STC and AAS adopted in the system will be introduced.

2.1 Physical Layer Description

Worldwide Interoperability of Microwave Access (WiMAX) is a technology based on the IEEE 802.16 specifications to enable the delivery of last mile wireless broadband access as an alternative to cable and DSL. WiMAX will provide fixed, nomadic, and portable mobile wireless broadband connectivity without the requirement for direct line-of-sight (LOS) with a base station. WiMAX provides metropolitan area network connectivity at speeds of up to 75 Mb/sec. WiMAX systems can be used to transmit signal as far as 30 miles. However, on the average a WiMAX base-station installation will likely cover between three to five miles [11].

WiMAX covers both LOS and NLOS applications in the 2-66 GHz frequencies. The PHY layer contains several forms of modulation and multiplexing to support different frequency range and application. Data rates determined by exact modulation and encoding schemes are shown in Table 2.1. The IEEE 802.16 standard was originally written to support several physical medium interfaces and it is expected that it will continue to develop and extend to support other PHY specifications. Hence, the modular nature of the standard is helpful in this aspect. For example, the first version of the standard only supported single carrier modulation. Since that time, OFDM has been added [12].

Table 2-1: Data rate for different modulations and code rates

Bandwidth (MHz)	Raw bit rate (Mb/s)		
	QPSK, CC3/4	16QAM, CC3/4	64QAM, CC3/4
6	7.5	15	22.5
7	8.7	17.5	26.1
20	24.4	48.8	73.2

In IEEE 802.16-2005, its applications are focused on mobile applications in the 2-6 GHz. Two multi-carrier modulation techniques are supported in 802.16-2005: OFDM with 256 carriers and OFDMA with 128, 512, 1024, or 2048 carriers.

In the following sections, we will introduce the main block diagrams of the transmitter architecture. We will put emphasis on physical layer description on OFDMA mode in IEEE 802.16-2005.

2.1.1 Randomizer

The randomization is performed on each burst of data on the DL and UL, which means that for each allocation of a data block, the randomizer shall be used independently. For RS and CC encoded data, padding will be added to the end of the transmission block, up to the amount of data allocated minus one byte, which shall be reserved for the introduction of a 0x00 tail byte by the FEC. The PRBS generator shall be $1 + X^{14} + X^{15}$ as shown in Figure 2-1. Each data byte to be transmitted shall enter sequentially into the randomizer. Preambles are not randomized.

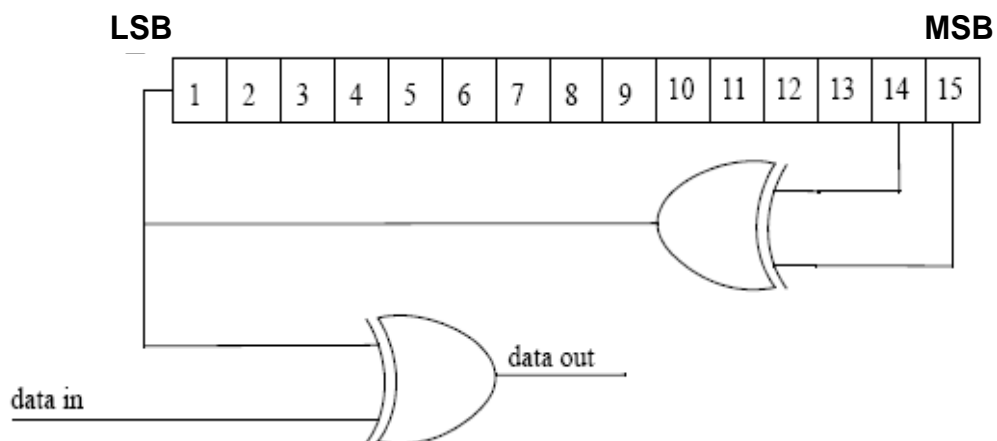


Figure 2-1: PRBS generator for randomizer

On the downlink, the randomizer shall be re-initialized at the start of each frame. In OFDMA mode, the randomizer shall be re-initialized with the sequence: [LSB]011011100010101[MSB]. At the start of subsequent bursts, the randomizer shall be initialized with the vector shown in Figure 2-2. The frame number used for initialization refers to the frame in which the DL burst is transmitted. The subchannel offset used for initialization refers to the allocated subchannels in which the DL burst is transmitted.

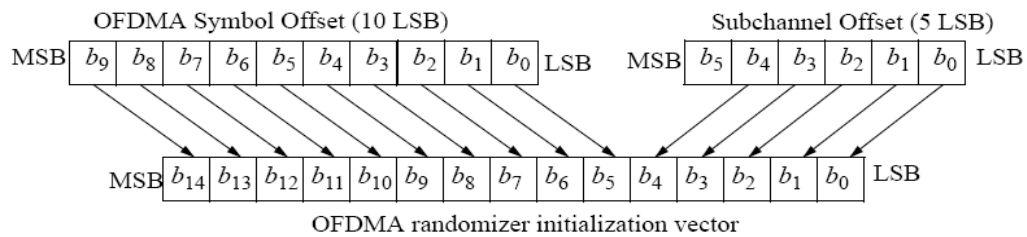


Figure 2-2: OFDMA randomizer DL initialization vector

2.1.2 Forward Error Correction

In OFDMA mode, the encoding is performed by passing the data in block format through a convolutional encoder. A single 0xFF tail byte is appended to the end of each burst after randomization. Each data block is encoded by the binary convolutional encoder, which shall have native rate of 1/2, a constraint length equal to 7, and shall use the generator depicted in Figure 2-3. Puncturing patterns and serialization order that shall be used to realize different code rates are defined in Table 2-2. Table 2-3 gives the data payload sizes and the code rates used for the different modulations.

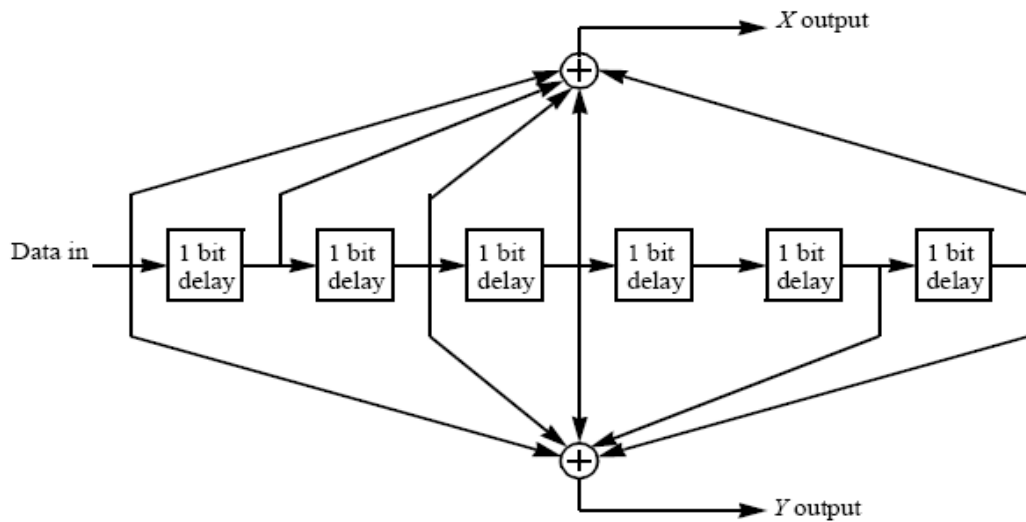


Figure 2-3: Convolutional encoder

Table 2-2: Puncturing patterns and orders to realize different code rates

	Code rates		
Rate	1/2	2/3	3/4
d_{free}	10	6	5
X	1	10	101
Y	1	11	110
XY	$X_1 Y_1$	$X_1 Y_1 Y_2$	$X_1 Y_1 Y_2 X_3$

Table 2-3: Useful data payload for a slot

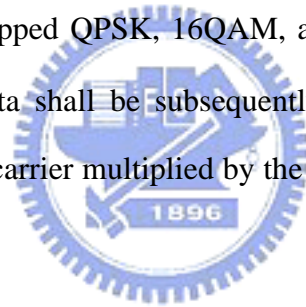
	QPSK		16 QAM		64 QAM		
Encoding rate	R=1/2	R=3/4	R=1/2	R=3/4	R=1/2	R=2/3	R=3/4
Data payload (bytes)	6						
		9					
	12		12				
	18	18		18	18		
	24		24			24	
		27					27
	30						
	36	36	36	36	36		

2.1.3 Interleaver

All encoded data bits shall be interleaved by a block interleaver with a block size corresponding to the number of coded bits over the allocated subchannels per OFDM symbol. The interleaver is defined by two step permutation. The first permutation ensures that adjacent coded bits are mapped onto nonadjacent subcarriers. The second permutation ensures that adjacent coded bits are mapped alternately onto less or more significant bits of the constellation, thus avoiding long runs of lowly reliable bits.

2.1.4 Modulator

After bit interleaving, the data are entered serially to the constellation mapper. For OFDMA mode, Gray-mapped QPSK, 16QAM, and 64QAM shall be supported. The constellation-mapped data shall be subsequently modulated onto all allocated data subcarriers and each subcarrier multiplied by the factor $2^{*(1/2 - w_k)}$ according the subcarrier index, k .



2.1.4.1 Pilot Modulation

Pilot subcarriers shall be inserted into each data burst in order to constitute the symbol and they shall be modulated according to their carrier location within the symbol. The PRBS generator depicted in Figure 2.4 shall be used to produce a sequence, w_k . The polynomial for the PRBS generator shall be $1 + X^9 + X^{11}$. For OFDMA mode, each pilot shall be transmitted with a boosting of 2.5 dB over the average power of each data tone. The pilot subcarriers shall be modulated according to (2-1):

$$\text{Re}\{c_k\} = \frac{8}{3} \left(\frac{1}{2} - w_k \right) \quad \text{and} \quad \text{Im}\{c_k\} = 0. \quad (2-1)$$

The pilot in DL preamble shall be modulated according to (2-2):

$$\begin{aligned} \text{Re}\{preablePilotsModulated\} &= 4 \cdot \sqrt{2} \cdot \left(\frac{1}{2} - w_k\right) \\ \text{Im}\{preablePilotsModulated\} &= 0 \end{aligned} \quad (2-2)$$

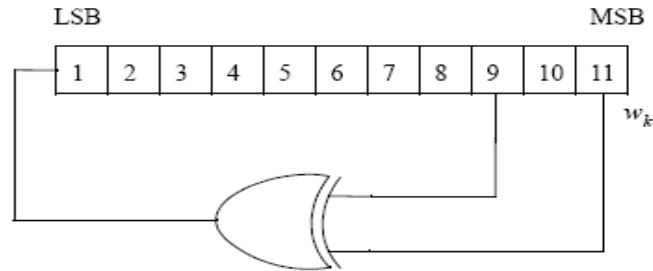


Figure 2-4: PRBS generator for pilot modulation

2.1.4.2 Preamble Structure

For OFDMA mode, the first symbol of the DL transmission is the preamble and the preamble subcarriers are divided into three carrier-sets. Those subcarriers are modulated using a boosted BPSK modulation with a specific PN code. There are three possible groups consisting of a carrier-set each that may be used by any segment. Each segment uses a preamble composed of a carrier-set out of the three available carrier-sets in the following manner: (In the case of segment 0 under 2048-FFT, the DC carrier will not be modulated at all and the appropriate PN will be discarded; therefore, DC carrier shall be always zero. For the preamble symbol of 2048-FFT, there will be 172 guard band subcarriers on the left side and the right side of the spectrum). For example, Figure 2-8 depicts the preamble of segment 1 for 2048-FFT.



Figure 2-5: Example of DL preamble for segment 1

2.2 Key Features of Scalable OFDMA

Although IEEE 802.16-2005 is generally perceived as the mobile version of the standard, in reality it serves the dual purpose of adding extensions for mobility and including new enhancements to the OFDMA physical layer. This new enhanced IEEE 802.16-2005 physical layer is now being referred as Scalable OFDMA (SOFDMA) and includes a number of important features for fixed, nomadic, and mobile networks. Because of these advantages, most of the industry will build their IEEE 802.16-2005 products using SOFDMA technology. However, the IEEE 802.16-2005 standard is not just for mobility. There are also many compelling reasons for using SOFDMA in fixed broadband wireless access (BWA) networks. In this section, we will focus on some key features of SOFDMA for mobile wireless applications [13], [14].

2.2.1 Scalable Channel Bandwidth

Scalability is one of the most important advantages of OFDMA. Spectrum resources for wireless broadband worldwide are still quite different in its allocation. With OFDMA subcarrier structure, it is designed to be able to scale to work in different channelization from 1.25 to 20 MHz to cope with varied worldwide requirements as efforts proceed to achieve spectrum harmonization in the longer term. The scalability is supported by adjusting FFT size according to the different channel bandwidth to fix the subcarrier frequency spacing. By fixing the subcarrier spacing

and symbol duration, the basic unit of physical resource is fixed. Therefore, the impact to higher layers is minimal when scaling the bandwidth.

The significant advantage from scalability is the flexibility of deployment. With the little modification to different air interfaces, OFDMA system can be deployed in various frequency bands to flexibly address the requirement for various spectrum allocation and usage model requirements. The OFDMA scalability parameters used in the thesis are listed in Table 2-4. The subcarrier spacing is fixed to 11.16 kHz and the symbol time is fixed to 89.6 μs . With the flexibility to support wider range bandwidth, OFDMA also enjoys high sector throughput, which allows more efficient multiplexing of data traffic, lower latency and better quality of service (QoS).

Table 2-4: OFDMA scalability parameters for different bandwidth

Parameters	Values				
Bandwidth (MHz)	1.25	2.5	5	10	20
Sampling frequency (MHz)	1.43	2.86	5.71	11.4	22.8
FFT size	128	256	512	1024	2048
Subcarrier spacing	11.16 KHz				
Useful symbol time (T _b)	89.6 μs				
CP duration	22.4 μs (T _b /4)				

2.2.2 Sub-channelization and Permutation

Active (data and pilot) subcarriers are grouped into subsets of subcarriers called subchannels. The OFDMA PHY supports sub-channelization in both DL and UL. The minimum frequency-time resource unit of sub-channelization is one slot, which is equal to 48 data tones. There are two major types of subcarriers permutation for

subchannelization: *diversity* and *contiguous*. The diversity permutation takes subcarriers pseudo-randomly to form a subchannel. The diversity permutations include DL & UL PUSC (Partial Usage of Subchannels), DL FUSC (Full Usage of Subchannels), and additional optional permutations. The contiguous permutation groups a block of adjacent sub-carriers to form a subchannel. The contiguous permutations include DL & UL AMC (Adaptive Modulation and Coding). With DL PUSC, for each pair of OFDM symbols, the usable subcarriers are grouped into *clusters* containing 14 adjacent subcarriers per symbol, with pilot and data allocations in each cluster in the even and odd symbols as shown in Figure 2-6. Other definitions of the PUSC subcarrier allocation are: one *subchannel* contains two clusters by one OFDMA symbol and one *slot* is one subchannel by two OFDMA symbols.

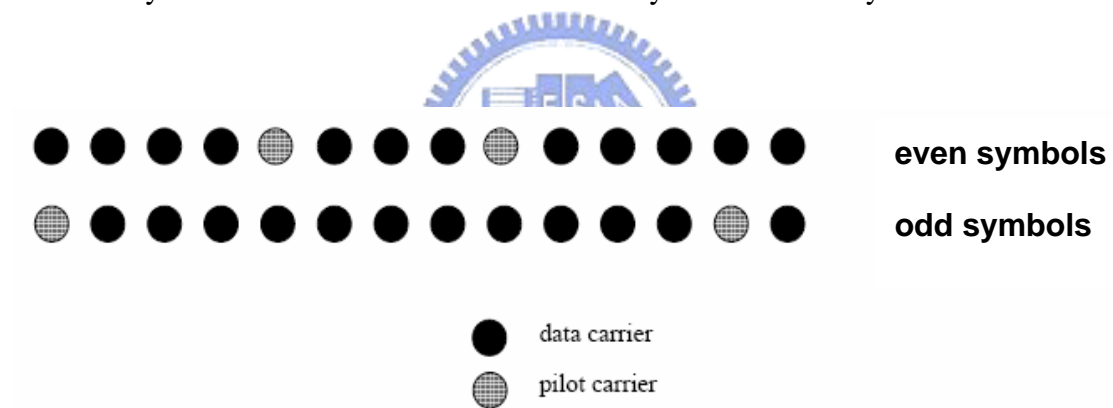


Figure 2-6: Cluster structure

Divide these clusters into several *Major Groups*. The allocation algorithm varies with FFT sizes. For each subchannel, subcarriers are distributed in some clusters that belong to its major group as shown in Figure 2.7. A subchannel contains 2 clusters and is comprised of 48 data subcarriers and 8 pilot subcarriers. Allocating subcarriers to subchannel in each major group is performed separately for each OFDMA symbol by first allocating the pilot carriers within each cluster, and then taking all remaining data carriers within the symbol and using the procedure described in (2-3):

$$subcarrier(k, s) = N_{subchannels} \cdot n_k + \{p_s[n_k \bmod N_{subchannels}] + DL_PermBase\} \bmod N_{subchannels} \quad (2-3)$$

where

$subcarrier(k, s)$ is the subcarrier index k in subchannel s

$N_{subchannels}$ is the number of subchannels in current partitioned major group

$n_k = (k + 13 \cdot s) \bmod N_{subcarriers}$

$N_{subcarriers}$ is the number of data subcarriers allocated to a subchannel

$p_s[j]$ is the series obtained by rotating basic permutation sequence cyclically to the left s times

The parameters vary with FFT sizes. Figure 2-8 shows an example of mapping OFDMA slots into subchannels and symbols in the DL PUSC.

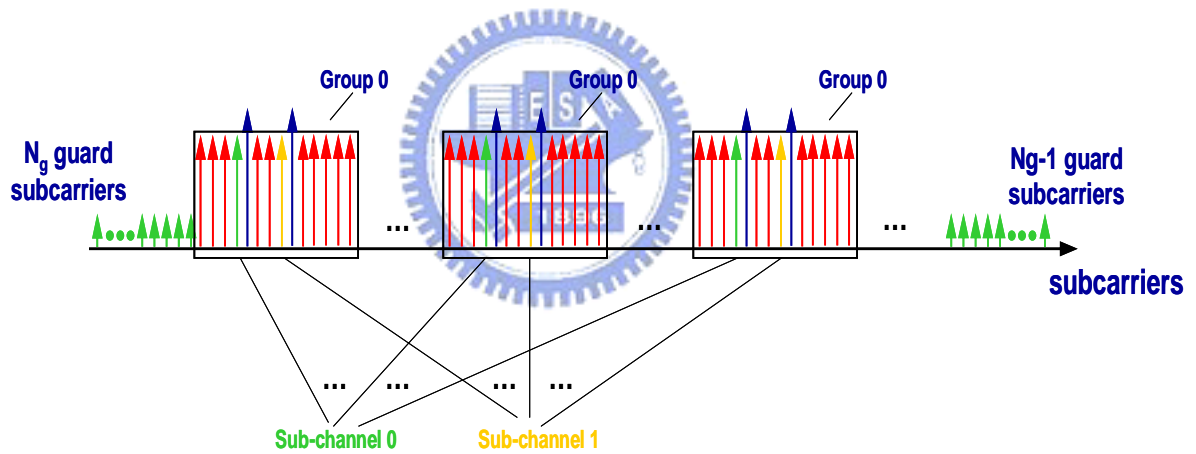


Figure 2-7: Allocated subcarriers into subchannels for PUSC

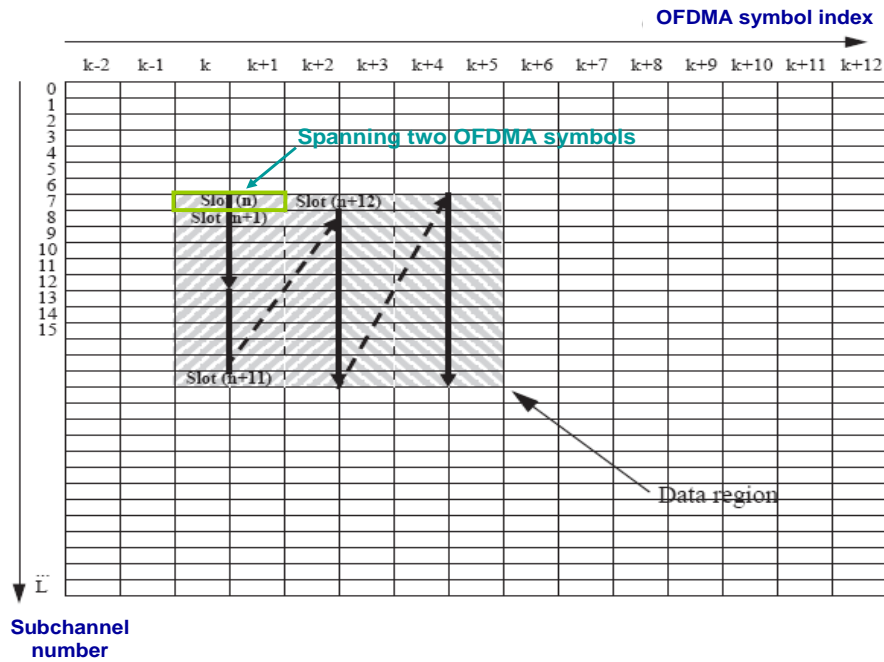


Figure 2-8: Example of mapping OFDMA slots to subchannels and symbols in DL

PUSC

Compared with the cluster structure for DL PUSC, a *tile* structure is defined for the UL PUSC whose format is shown in Figure 2-9. The slot is comprised of 48 data subcarriers and 24 pilot subcarriers in 3 OFDM symbols.

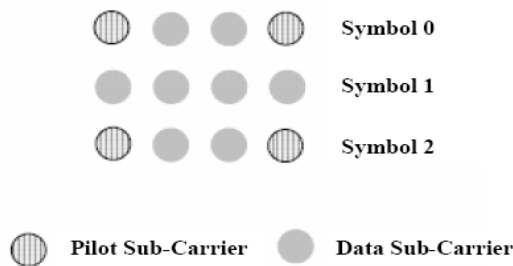


Figure 2-9: Description of a UL PUSC tile

FUSC achieves full diversity by spreading tones over entire band. The symbol structure is constructed using pilots, data, and zero subcarriers. The symbol is first allocated with the appropriate pilots and with zero subcarriers, and then all the

remaining subcarriers are used as data subcarriers. To allocate the data subchannels, the remaining subcarriers are partitioned into groups of contiguous subcarriers. Each subchannel consists of one subcarrier from each of these groups as shown in Figure 2-10. The number of groups is therefore equal to the number of subcarriers per subchannel. The exact partitioning into subchannels is according to the same procedure as (2-3).

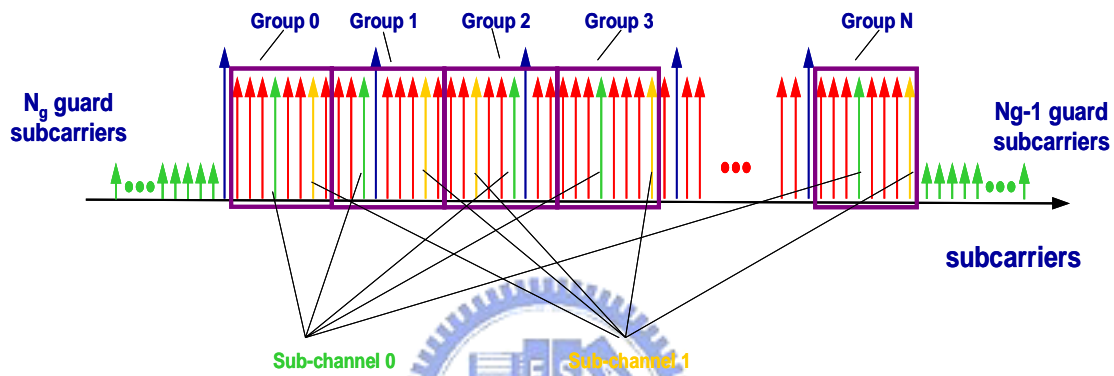


Figure 2-10: Allocated subcarriers into subchannels for FUSC

The contiguous permutation groups a block of adjacent subcarriers to form a subchannel, such as DL AMC and UL AMC. As shown in Figure 2-11, a bin consists of 9 adjacent subcarriers in a symbol, with 8 tones for data and one assigned for a pilot. A *slot* in AMC is defined as a collection of bins of the type ($N \times M = 6$), where N is the number of adjacent bins and M is the number of adjacent symbols. Thus 4 different ways of defining a slot are (6 bins, 1 symbol), (3 bins, 2 symbols), (2 bins, 3 symbols), (1 bin, 6 symbols). AMC permutation enables multi-user diversity by choosing the sub-channel with the best channel frequency response.

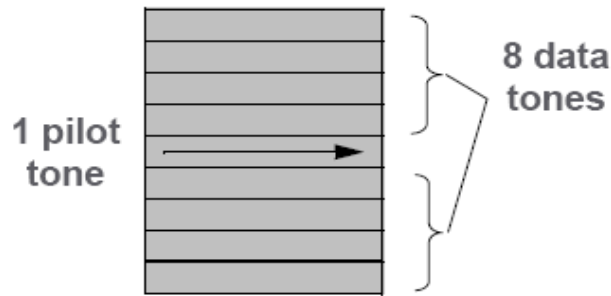


Figure 2-11: AMC bin structure

In general, diversity subcarrier permutations perform well in mobile applications while contiguous subcarrier permutations are well suited for fixed, portable, or low mobility environments. These options enable the system designer to trade-off mobility for throughput.

2.2.3 Fractional Frequency Reuse

In OFDMA mode, users operate on subchannels which only occupy a small fraction of the channel bandwidth and the cell edge interference problem can be easily solved by reconfiguration of the subchannel usage without resorting to traditional frequency planning. In mobile applications, the flexible subchannel reuse is facilitated by subchannel segmentation and permutation zone. A segment is a subdivision of the available OFDMA subchannels (one segment may include all subchannels). Permutation Zone is a number of contiguous OFDMA symbols in DL or UL that use the same permutation. The DL or UL subframe may contain more than one permutation zone.

The subchannel reuse pattern can be configured so that users close to the base station operate on the zone with all subchannels available. While for the edge users, each cell and sector operates on the zone with a fraction of all subchannels available.

In Figure 2-11, F1, F2 and F3 are different sets of subchannels in the same frequency channel. With this configuration, the full load frequency reuse of one is maintained for center users to maximize spectral efficiency while fractional frequency reuse is achieved for edge users to improve edge user connection quality and throughput. The subchannel reuse planning can be dynamically optimized across sectors or cells based on network load and interference conditions on a frame by frame basis. All the cells and sectors therefore, can operate on the same frequency channel without the requirement for frequency planning.

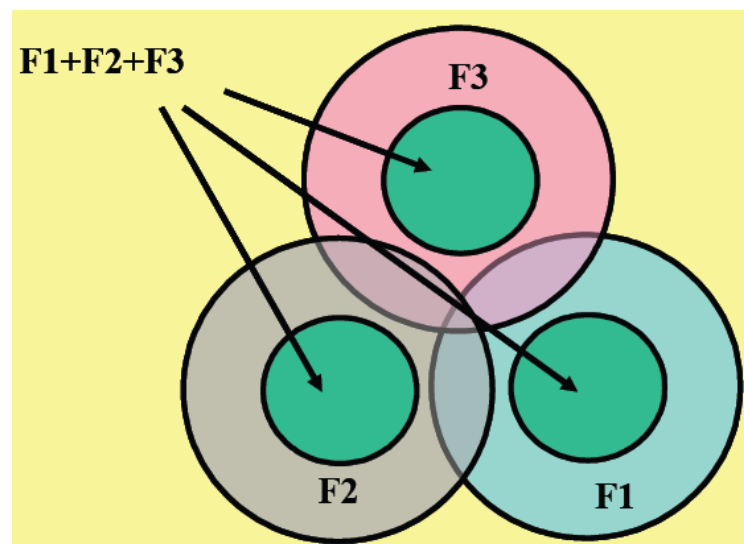


Figure 2-12: Description of fractional frequency reuse

2.3 Transmit Techniques

In order to increase the range and reliability of WiMAX systems, the WiMAX standard supports optional multiple-antenna techniques such as Alamouti Space-Time Coding (STC), Adaptive Antenna Systems (AAS) and Multiple-Input Multiple-Output (MIMO) systems.

There are several advantages to using multiple-antenna technology over

single-antenna technology:

- **Array Gain:** This is the gain achieved by using multiple antennas so that the signal adds coherently.

- **Diversity Gain:** This is the gain achieved by utilizing multiple paths so that the probability that any one path is bad does not limit performance. Effectively, diversity gain refers to techniques at the transmitter or receiver to achieve multiple “looks” at the fading channel. These schemes improve performance by increasing the stability of the received signal strength in the presence of wireless signal fading. Diversity may be exploited in the spatial (antenna), temporal (time), or spectral (frequency) dimensions.

- **Co-channel Interference Rejection (CCIR):** This is the rejection of signals by making use of the different channel response of the interferers.

2.3.1 Transmit Diversity: Space-Time Coding

In order to increase the rate and range of the modem, there are several considerations. Generally, BS can bear more cost and complexity than SS, so multiple-antenna techniques are a good option at BS, also called transmit diversity. Among various transmit diversity schemes, STC is the most popular scheme with the feature of open loop (i.e., no feedback signaling is required) as channel information is not required at the transmitter. Therefore we will focus on the scheme of STC with 2 transmit antennas in this section as shown in Figure 2-13.

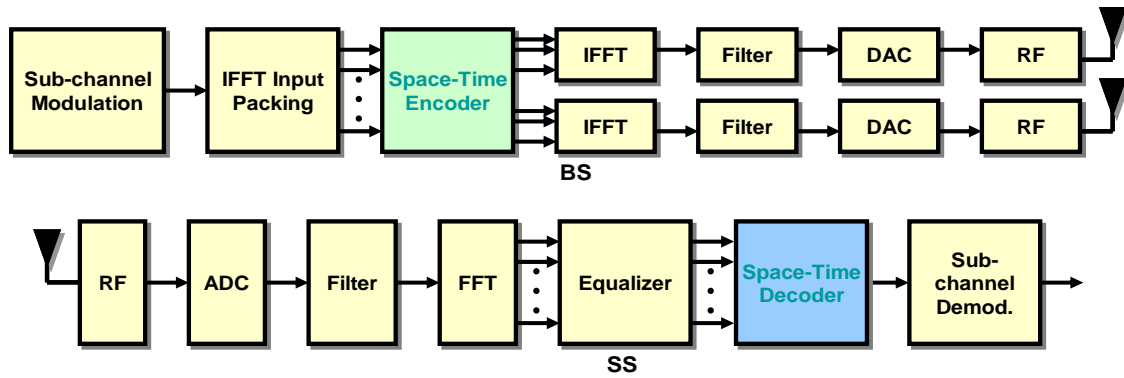


Figure 2-13: Block diagram of STC

The space-time block coding scheme was first discovered by Alamouti for two transmit antennas. Symbols transmitted from those antennas are encoded in both space and time in a simple manner to ensure that transmissions from both the antennas are orthogonal to each other. This would allow the receiver to decode the transmitted information with a slight increment in the computational complexity.

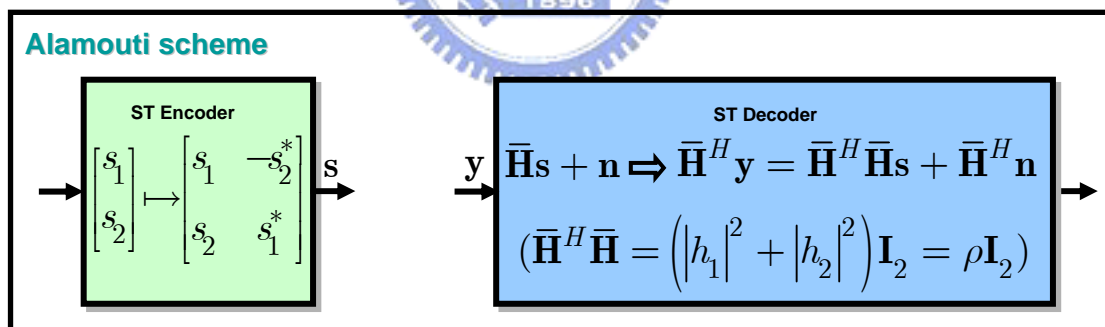


Figure 2-14: Illustration of Alamouti scheme

Figure 2-14 shows the operation of Alamouti scheme. The input symbols to the space-time block encoder are divided into groups of two symbols. At a given symbol period, the encoder takes a block of two modulated symbols s_1 and s_2 in each encoding operation and maps them to the transmit antennas according to a code matrix given by

$$\mathbf{s} = \begin{bmatrix} s_1 & -s_2^* \\ s_2 & s_1^* \end{bmatrix}. \quad (2-4)$$

The encoder outputs are transmitted in two consecutive transmission periods from two transmit antennas. Let h_1 and h_2 be the channel gains from the first and second transmit antennas to the only one receiver antenna. Assume that h_1 and h_2 are scalar and constant over two consecutive symbol periods. The received signals in two consecutive symbol periods, denoted as r_1 and r_2 , can be expressed as

$$\begin{aligned} r_1 &= h_1 s_1 + h_2 s_2 + n_1 \\ r_2 &= -h_1 s_2^* + h_2 s_1^* + n_2 \end{aligned}, \quad (2-5)$$

where n_1 and n_2 are AWGN noise modeled as identical independent distributed (i.i.d.) complex Gaussian random variables with zero mean and power spectral density $N_0/2$ for each dimension. The above equation can be rewritten in a matrix form as

$$\mathbf{r} = \begin{bmatrix} r_1 \\ r_2^* \end{bmatrix} = \underbrace{\begin{bmatrix} h_1 & h_2 \\ (h_2)^* & -(h_1)^* \end{bmatrix}}_{\bar{\mathbf{H}}} \underbrace{\begin{bmatrix} s_1 \\ s_2 \end{bmatrix}}_{\mathbf{s}} + \underbrace{\begin{bmatrix} n_1 \\ n_2^* \end{bmatrix}}_{\mathbf{n}} = \bar{\mathbf{H}} \cdot \mathbf{s} + \mathbf{n}. \quad (2-6)$$

Since the channel matrix $\bar{\mathbf{H}}$ is unitary, i.e. $\bar{\mathbf{H}}^H \bar{\mathbf{H}} = \rho \cdot \mathbf{I}_2$, where $\rho = |h_1|^2 + |h_2|^2$, the ML decoder can perform an MRC operation on the modified signal vector $\tilde{\mathbf{r}}$ given by

$$\begin{aligned} \tilde{\mathbf{r}} &= \bar{\mathbf{H}}^H \cdot \mathbf{r} = \rho \cdot \mathbf{s} + \underbrace{\bar{\mathbf{H}}^H \cdot \mathbf{n}}_{\tilde{\mathbf{n}}}. \\ &= \rho \cdot \mathbf{s} + \tilde{\mathbf{n}} \end{aligned} \quad (2-7)$$

Therefore, we can obtain the space-time decoded vector \mathbf{s} .

For OFDMA mode, STC coding is done on all data subcarriers that belong to an STC coded burst in the two consecutive OFDMA symbols. Pilot subcarriers are not encoded and are transmitted from either antenna 0 or antenna 1. In PUSC, the pilot

allocation to cluster is changed as shown in Figure 2-15. The pilot locations change in period of 4 symbols to accommodate two antennas transmission with the same estimation capability.

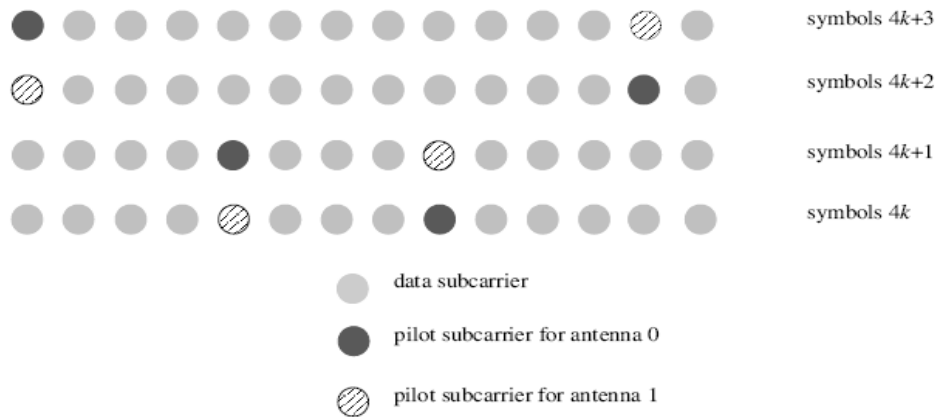


Figure 2-15: Cluster structure for STC PUSC using 2 Antennas

2.3.2 Transmit Beamforming: Adaptive Antenna System



Future wireless communication systems aim at providing higher data rates with better link quality subject to being *interference limited*. Smart antenna technology is one of the most promising technologies for increasing both system coverage and capacity as shown in Figure 2-16. AAS, although an optional feature, through the use of more than one antenna elements at BS, can significantly improve range and capacity by adapting the antenna pattern and concentrating its radiation to each individual user. There are several advantages of using beamforming:

- Increase spectral efficiency proportional to the number of antenna elements
- Realize an inter-cell frequency reuse of one and an in-cell reuse factor proportional to the number of antenna elements
- Reduce interference by steering nulls in directions of co-channel interferers

- Increase SNR of certain subscribers and steer nulls to others that can enable bursts to be concurrently transmitted to spatially separated users.

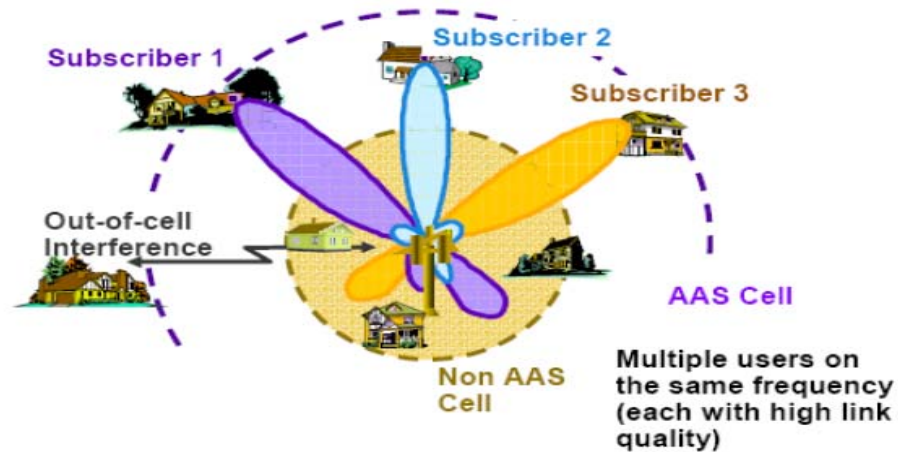


Figure 2-16: Illustration of AAS

First, the generalized AAS zone allocation is introduced as shown in Figure 2-17. The frame is divided into two parts: the first part is allocated to the non-AAS users and the second part (called AAS zone) is allocated to the AAS users. This allows a mixture of non-AAS and AAS users to be supported by the same BS. The BS can dynamically allocate capacity to non-AAS and AAS traffic. The SS without AAS capability will ignore the traffic in the AAS zone.

Figure 2.18 shows the AAS zone structure in OFDMA mode. AAS_DLFP in an AAS zone is preceded by an AAS DL preamble of one symbol duration. All other data bursts within an AAS zone have a preamble whose duration is specified in AAS_DL_IE. AAS_DLFP provides a robust transmission of required BS parameters to enable SS access allocation. Each AAS_DLFP requires not carry the same information. Different beams may be used within the AAS diversity map zone. For

OFDMA mode, REP-RSP MAC message shall be sent by SS in response to a REP-REQ message from the BS to report estimation of the mean DL CINR (carrier-to-interference-and-noise ratio).

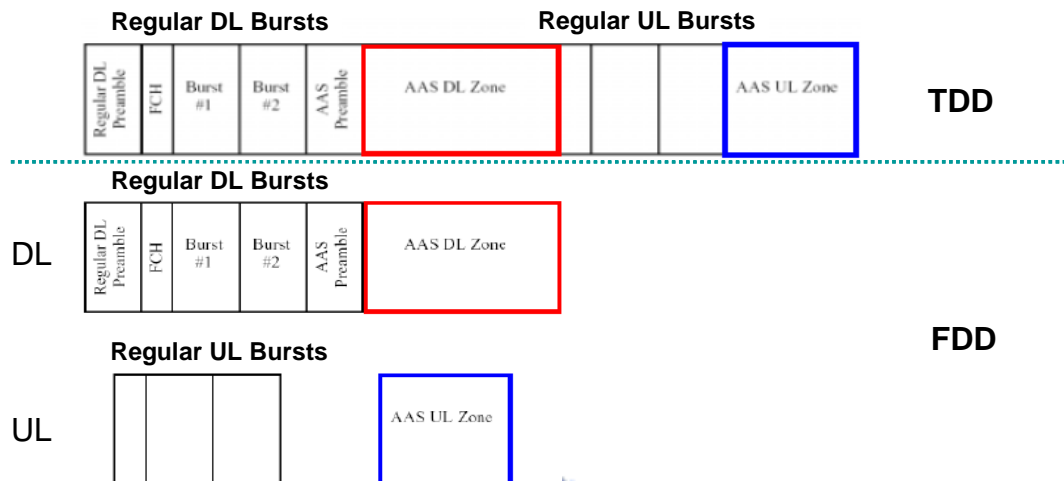


Figure 2-17: Generalized AAS zone allocation

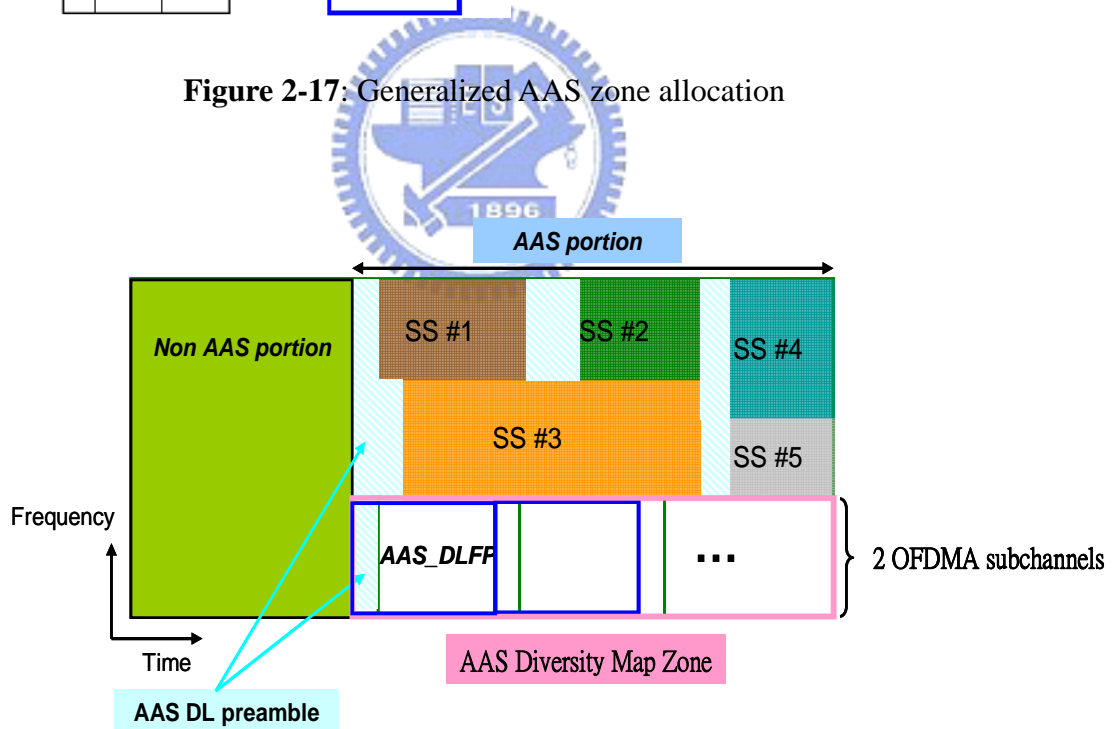


Figure 2-18: AAS zone structure in OFDMA mode

2.4 Summary

Specification of IEEE 802.16-2005 system has been introduced in this chapter.

The key features of scalable OFDMA in IEEE 802.16-2005 is also described to see the enhanced structure in mobile environment. We also introduce some key transmit techniques and their operations. By using these transmit techniques, the capacity and range of the system can be improved significantly.



Chapter 3

Channel Estimation for Mobile WiMAX System

The use of multi-amplitude schemes in wireless OFDM systems requires the tracking of the fading radio channel. In real situations, channel estimation should be done before data detection to avoid bad distortion of the channel. In this chapter, channel estimation and interpolation schemes are introduced. First, three channel models corresponding to static or mobile environments are introduced in Section 3.1. Then, in Section 3.2, conventional least square (LS) and minimum mean square error (MMSE) channel estimation schemes [15] with several interpolation approaches [16] are introduced. In mobile environment, the need for the estimate of channel impulse response in time domain leads us to the time domain LS channel estimator [17]. The channel estimates can be further adopted to do the ICI mitigation in Chapter 4.

3.1 Channel Model

Wireless propagation channels have been studied for more than 50 years, and a large number of channel models are already available. The signal that has propagated through a wireless channel consists of multiple echoes of the originally transmitted signals; this phenomenon is known as multipath propagation. The different multipath components are characterized by different attenuations and delays. The correct modeling of the parameters describing the multipath components is the key point of channel modeling.

In first generation systems, a super-cell architecture is used where the base station and subscriber station are in LOS condition and the system uses a single cell with no co-channel interference. For second generation systems, a scalable multi-cell architecture with NLOS conditions becomes necessary. In WiMAX system, the wireless channel is characterized by:

- Path loss (including shadowing)
- Multipath delay spread
- Fading characteristics
- Doppler spread

The main channel models were considered here: Stanford University Interim (SUI) channel models [18], International Telecommunication Union (ITU) channel models [19] and Spatial Channel Model (SCM) channel models [20]. Each channel model was parameterized in order to best fit the particular channel characteristics.

3.1.1 SUI Channel Model for Fixed Wireless

Application

SUI channel models were proposed in [18] to model a statistic environment in

IEEE 802.16-2004. There are many possible combinations of parameters to obtain different channel descriptions. A set of 6 typical channels were selected for the three terrain types that are typical of the continental US. The channel parameters are related to terrain type, delay spread, and antenna directionality and each channel model has three taps with distinct K-factor and average power. Table 3-1 shows an example of time domain attribute of the SUI-3 channel, which is chosen to evaluate the proposed algorithm.

Table 3-1: Parameters of SUI-3 channel models

SUI – 3 Channel				
	Tap 1	Tap 2	Tap 3	Units
Delay	0	0.4	0.9	μs
Power (omni ant.)	0	-5	-10	dB
90% K-fact. (omni)	1	0	0	
75% K-fact. (omni)	7	0	0	
Doppler	0.4	0.3	0.5	Hz
Antenna Correlation:		$\rho_{ENV} = 0.4$		
Gain Reduction Factor:		GRF = 3 dB		
Normalization Factor:		$F_{omni} = -1.5113$ dB, $F_{30^\circ} = -0.3573$ dB		

Multipath Delay Profile

Due to the scattering environment, the channel has a multipath delay profile. It is characterized by τ_{rms} (RMS delay spread of the entire delay profile) which is defined as

$$\tau_{rms}^2 = \sum_j P_j \tau_j^2 - (\tau_{avg})^2 \quad (3-1)$$

where

$$\tau_{avg} = \sum_j P_j \tau_j,$$

τ_j is the delay of the j th delay component of the profile and P_j is given by

P_j = (power in the j th delay component) / (total power in all components)

RMS delay spread

A delay spread model was based on a large body of published reports. It was found that the RMS delay spread follows lognormal distribution and that the median of this distribution grows as some power of distance. The model was developed for rural, suburban, urban, and mountainous environments. The model is of the following form

$$\tau_{rms} = T_1 d^\varepsilon y \quad (3-2)$$

where τ_{rms} is the RMS delay spread, d is the distance in km, T_1 is the median value of τ_{rms} at $d = 1$ km, ε is an exponent that lies between 0.5 ~ 1.0, and y is a lognormal variant. Depending on the terrain, distance, antenna directivity and other factors, the RMS delay spread values can span from very small values (tens of nanoseconds) to large values (microseconds).

Fading distribution, K-factor

The narrow band received signal fading can be characterized by a Ricean fading. The key parameter of this distribution is the K-factor, defined as the ratio of the “fixed” component power and the “scatter” component power. The narrow band K-factor distribution was found to be lognormal, with the median as a simple function of season, antenna height, antenna beamwidth and distance. The model for the K-factor (in linear scale) is as follows:

$$K = F_s F_h F_b K_o d^\gamma u \quad (3-3)$$

where

F_s is a season factor; $F_s = 1.0$ in summer; 2.5 in winter

F_h is the received antenna height factor

F_b is the beamwidth factor

K_o and γ are regression coefficients

u is a lognormal variable which has 0 dB mean and a standard deviation of 8 dB.

Using this model, one can observe that the K-factor decreases as the distance increases and as antenna beamwidth increases.

Doppler spectrum

The random components of the coefficients generated in the previous paragraph have a white spectrum since they are independent of each other. The SUI channel model defines a specific power spectral density (PSD) function for these scatter component channel coefficients called “rounded” PSD which is given as

$$S(f) = \begin{cases} 1 - 1.72f_0^2 + 0.785f_0^4 & |f_0| \leq 1 \\ 0 & |f_0| > 1 \end{cases} \quad (3-4)$$

where $f_0 = \frac{f}{f_m}$. In fixed wireless channels the shape of the spectrum is therefore different than the classical Jake’s spectrum for mobile channels. Figure 3-1 shows that its shape of Doppler spectrum is convex.

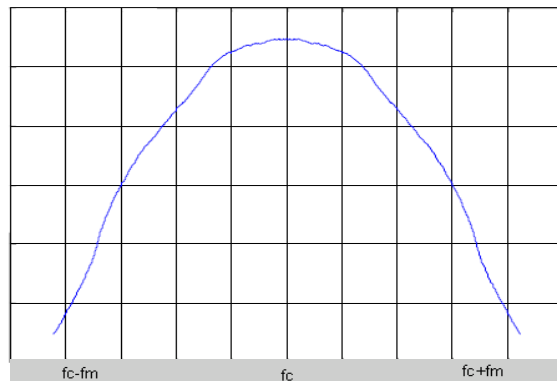


Figure 3-1: Doppler spectrum of SUI channel models

Antenna correlation

The SUI channel models define an antenna correlation, which has to be

considered if multiple transmit or receive elements, i.e. multiple channels, are being simulated. Antenna correlation is commonly defined as the envelope correlation coefficient between signals transmitted at two antenna elements. The received baseband signals are modeled as two complex random processes $X(t)$ and $Y(t)$ with an envelope correlation coefficient of

$$\rho_{env} = \left| \frac{E \{ (X - E \{X\})(Y - E \{Y\})^* \}}{\sqrt{E \{ |X - E \{X\}|^2 \} E \{ |Y - E \{Y\}|^2 \}}} \right| \quad (3-5)$$

Note that this is not equal to the correlation of the envelopes of two signals, a measure that is also used frequently in cases where no complex data is available.

Antenna gain reduction factor

The use of directional antennas requires to be considered carefully. The gain due to the directivity can be reduced because of the scattering. The effective gain is less than the actual gain. This factor should be considered in the link budget of a specific receiver antenna configuration.

Denote ΔG_{BW} as the Gain Reduction Factor. This parameter is a random quantity which dB value is Gaussian distributed with a mean μ_{grf} and a standard deviation σ_{grf} given by

$$\mu_{grf} = -(0.53 + 0.1I) \ln(\beta / 360) + (0.5 + 0.04I)(\ln(\beta / 360))^2 \quad (3-6)$$

$$\sigma_{grf} = -(0.93 + 0.02I) \ln(\beta / 360) \quad (3-7)$$

where

β is the beamwidth in degrees

$I = 1$ for winter and $I = -1$ for summer

In the link budget computation, if G is the gain of the antenna (dB), the effective

gain of the antenna equals $G - \Delta G_{BW}$. For example, if a 20-degree antenna is used, the mean value of ΔG_{BW} would be closed to 7 dB.

3.1.2 ITU Channel Model for Mobile Wireless

Application

As we know, for fixed wireless application such as IEEE 802.16-2004, the SUI channel models are recommended for simulation. However, for mobile wireless application like IEEE 802.16-2005, the recommendatory channel model is not proposed at present. Here we choose International Telecommunication Union (ITU) channel model [19] for mobile and fixed use.

ITU channel model is a measurement based channel model proposed for the 3GPP WCDMA system. Delay and average power of each multipath for the ITU channel models are summarized in Table 3-2. Four or six multipath signals are generated in the wireless channel depending on the channel type as shown in Table 3-2 respectively. The ITU channel model can be modeled as

$$w(t) = \sum_{n=1}^N \sqrt{p_n} g_n(t) z(t - \tau_n) \quad (3-8)$$

where $z(t)$ and $w(t)$ denote the complex low pass representations of the channel input and output respectively, p_n is the strength of the n th weight and $g_n(t)$ is the complex Gaussian process weighting the n th replica.

Table 3-2: Parameters of ITU channel models

Channel Profile \ Multipath		M1	M2	M3	M4	M5	M6
Pedestrian A ($M = 4$)	Delay (ns)	0	110	190	410	NA	NA
	Power (dB)	0	-9.7	-19.2	-22.8		
Pedestrian B ($M = 6$)	Delay (ns)	0	200	800	1200	2300	3700
	Power (dB)	0	-0.9	-4.9	-8.0	-7.8	-23.9
Vehicular A ($M = 6$)	Delay (ns)	0	310	710	1090	1730	2510
	Power (dB)	0	-1.0	-9.0	-10.0	-15.0	-20.0
Vehicular B ($M = 6$)	Delay (ns)	0	300	8900	12900	17100	20000
	Power (dB)	-2.5	0	-12.8	-10.0	-25.2	-16.0

As shown in Table 3-2, ITU channel model includes two environments. For the pedestrian test environment, this environment is characterized by small cells and low transmit power. Base stations with low antenna height are located outdoors, and pedestrian users are located on streets, inside buildings or residences. Its path loss is defined by

$$L = 40 \log_{10} R + 30 \log_{10} f + 49 \quad (\text{dB}), \quad (3-9)$$

where R denotes the separation (km) between the base station and the mobile station and f is carrier frequency.

For vehicular environment, it is characterized by large cells and higher transmit power. The model is applicable for in urban and suburban areas outside the high rise core where the buildings are of nearly uniform height. Its path loss is written as

$$L = 40 \left(1 - 4 \times 10^{-3} \Delta h_b\right) \log_{10} R - 18 \log_{10} \Delta h_b + 21 \log_{10} f + 80 \quad (3-10)$$

where

R is the separation (km) between base station and mobile station

f is carrier frequency

Δh_b is base station antenna height (m), measured from the average rooftop level
The path loss model is valid for a range of Δh_b from 0 to 50 m.

The ITU channel model uses Doppler spectrum of classical Jake's spectrum. As shown in Figure 3-2, the Doppler spectrum is concave.

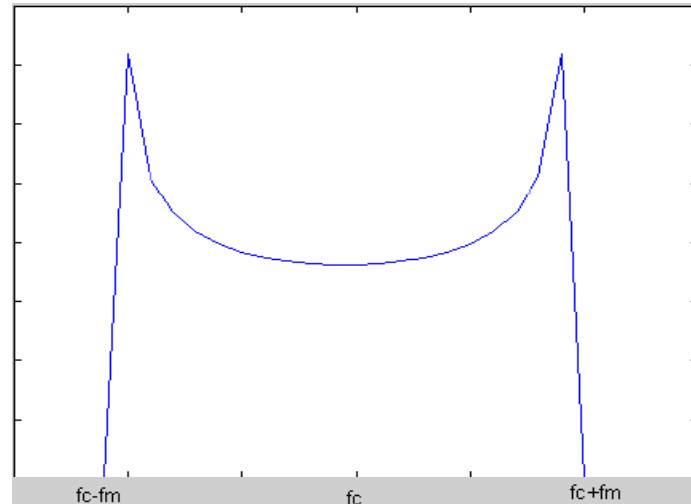


Figure 3-2: Doppler spectrum of ITU channel models

3.1.3 SCM Channel Model for Mobile MIMO

Wireless Application

Spatial Channel Model (SCM) channel model [20] is the channel model of third Generation Partnership Project (3GPP), which focuses on fixed and mobile MIMO wireless application. It is a detailed system level model for simulating urban micro-cell, urban macro-cell and suburban macro-cell fading environments. The SCM model considers N cluster of scatterers. Each cluster corresponds to a resolvable path. Within a resolvable path (cluster), there are M unresolvable subpaths. A simplified plot of the model is shown in Figure 3-3.

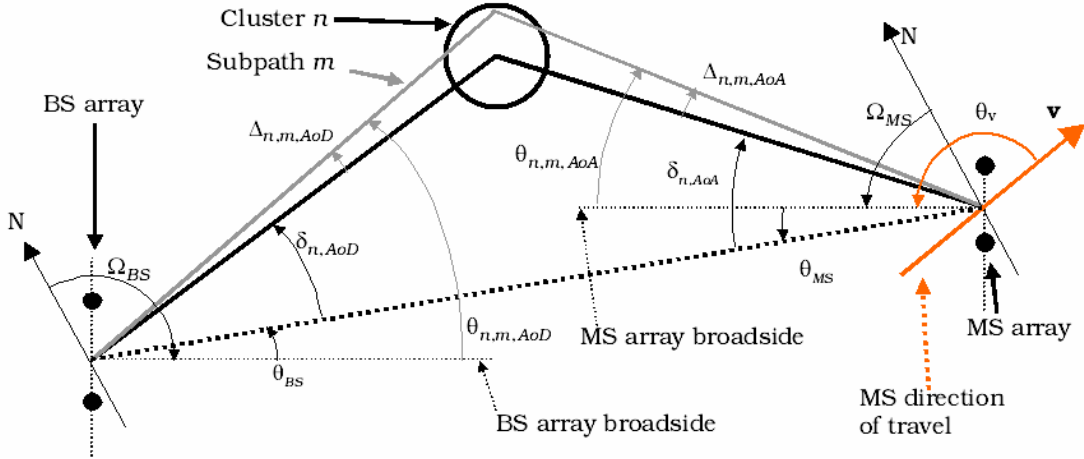


Figure 3-3: BS and MS angular parameters in SCM specification

For a N_T element linear BS array and a N_R element linear MS array, the channel coefficients of one of the N multipath components are given by a $N_R \times N_T$ matrix of complex amplitudes. Assuming omnidirectional antenna elements are employed at the BS and MS and neglecting pathloss and shadowing, the channel impulse response for the l th path between the s th transmit and u th receive antenna can be written as

$$h_{u,s,n}(t) = \sqrt{\frac{P_n}{M}} \sum_{m=1}^M \left\{ \begin{array}{l} \exp \left[j \left(k d_s \sin(\theta_{n,m,AOD}) + \phi_{n,m} \right) \right] \times \\ \exp \left[j k d_u \sin(\theta_{n,m,AOA}) \right] \times \\ \exp \left[j k \|\mathbf{v}\| \cos(\theta_{n,m,AOA} - \theta_v) t \right] \end{array} \right\}. \quad (3-11)$$

where $j = \sqrt{-1}$, k is the wave number $2\pi/\lambda$, λ is the carrier wavelength in meters, P_n is the power of the n th path, M is the number of subpaths per-path, d_s is the distance in meters from BS antenna element s to the reference ($s = 1$) antenna, d_u is the distance in meters from MS antenna element u to the reference ($u = 1$) antenna, $\|\mathbf{v}\|$ is the magnitude of the MS velocity vector, $\theta_{n,m,AOA}$ is the Angle of Arrival

(AOA) for the m th subpath of the n th path with respect to the MS broadside and $\theta_{n,m,AOD}$ is the Angle of Departure (AOD) for the m th subpath of the n th path with respect to the BS broadside. The details of the generation of relevant parameters are given in [20].

3.2 Channel Estimation

This section describes channel estimation schemes to recover the channel frequency response. Recall that the frame structure of OFDMA in IEEE-802.16 is described as with certain pilot subcarriers in subbands for the both preamble and the data frames, as described in 2.1.4. We have to develop the pilot-based channel estimation which is introduced in [21] with the system structure shown in Figure 3-4.

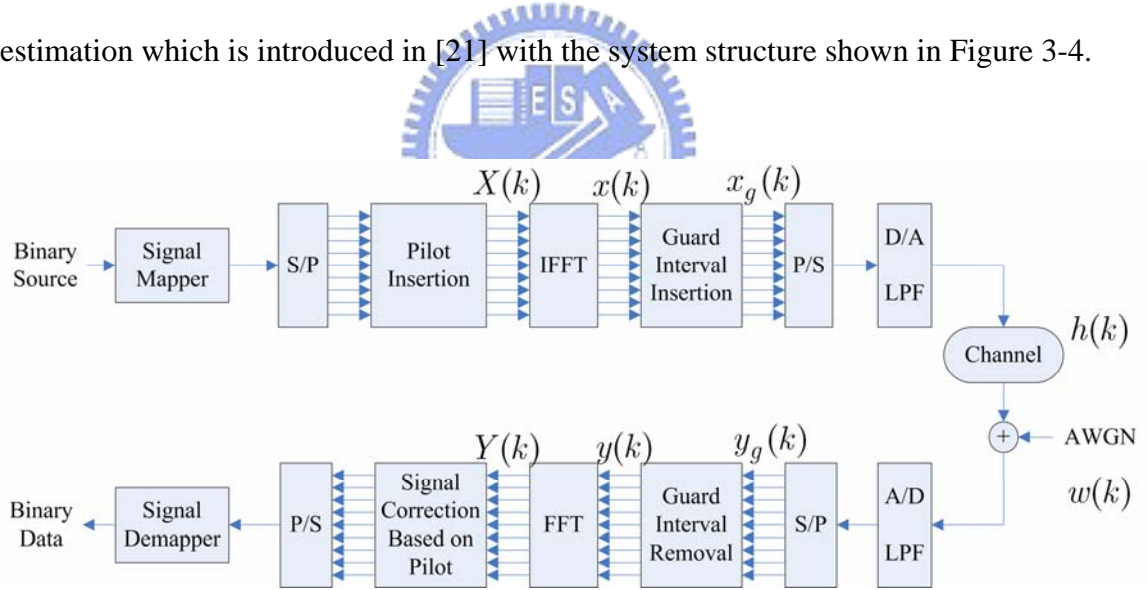


Figure 3-4: Baseband model of a typical pilot-based system

For the discrete baseband equivalent system shown in Figure 3-4, we assume perfect timing synchronization in this thesis. The binary information data are grouped and mapped into multi-amplitude-multi-phase signals, which can be chosen as QPSK, 16-QAM, and 64-QAM in IEEE 802.16 OFDMA. After pilot insertion described in

Figure 2-6, the modulated data $\mathbf{X} = [X(0), X(1), \dots, X(N-1)]^T$ are transformed and multiplexed into time domain response $\mathbf{x} = [x(0), x(1), \dots, x(N-1)]^T$ using the inverse discrete fourier transform (IDFT):

$$\mathbf{x} = \mathbf{F}^H \mathbf{X}, \quad (3-12)$$

where N is the number of subcarriers and \mathbf{F} is the DFT matrix

$$\mathbf{F} = \begin{bmatrix} W_N^{00} & \dots & W_N^{0(N-1)} \\ \vdots & \ddots & \vdots \\ W_N^{(N-1)0} & \dots & W_N^{(N-1)(N-1)} \end{bmatrix} \quad (3-13)$$

with

$$W_N^{nk} = \frac{1}{\sqrt{N}} e^{-j2\pi \frac{nk}{N}}. \quad (3-14)$$

The guard interval is then inserted to prevent possible inter-symbol interference (ISI) in OFDM systems, and the resultant samples $\{x_g(n)\}$ are

$$x_g(n) = \begin{cases} x(N+n), & n = -G, \dots, -1 \\ x(n), & n = 0, 1, \dots, N-1 \end{cases}, \quad (3-15)$$

where G is the number of samples in the guard interval. The transmitted signal is then sent to a multi-path fading channel. The received signal can be represented by

$$y_g(k) = x_g(k) \otimes h(k) + n(k), \quad (3-16)$$

where $h(k)$ is the impulse response of channel and $n(k)$ is the additive white Gaussian noise (AWGN). The channel impulse response $h(k)$ can be expressed as:

$$h(k) = \sum_{i=0}^{L-1} g_i \times \delta(k - \tau_i), \quad (3-17)$$

where L is the total number of propagation paths, g_i is the complex impulse

response of the i th path, and τ_i is the i th-path delay time normalized by sampling time.

After removing the guard interval from $y_g(k)$, the received signal $\mathbf{y} = [y(0), y(1), \dots, y(N-1)]^T$ can be expressed in matrix form

$$\mathbf{y} = \bar{\mathbf{h}}\mathbf{F}^H\mathbf{X} + \mathbf{w}, \quad (3-18)$$

where

$$\bar{\mathbf{h}} = \begin{bmatrix} h(0) & \mathbf{0} & h(G) & \dots & h(1) \\ h(1) & h(0) & \mathbf{0} & h(G) & \dots \\ \vdots & \vdots & \ddots & \dots & \dots \\ \mathbf{0} & h(G) & \dots & h(0) & \mathbf{0} \end{bmatrix} \quad (3-19)$$

is the channel matrix which represents the circular convolution of (3.16). Then, the signals are sent to the DFT block to demultiplex the multicarrier signals:

$$\mathbf{Y} = \mathbf{F}\mathbf{y} = \mathbf{F}\bar{\mathbf{h}}\mathbf{F}^H\mathbf{X} + \mathbf{F}\mathbf{w}. \quad (3-20)$$

Set

$$\begin{aligned} \mathbf{H} &= \mathbf{F}\mathbf{h} \\ &= [H(0), H(1), \dots, H(N-1)]^T, \end{aligned} \quad (3-21)$$

since the channel matrix $\bar{\mathbf{h}}$ is Toeplitz and \mathbf{F} is unitary, $\mathbf{F}\bar{\mathbf{h}}\mathbf{F}^H$ can be simplified [22], [23] as

$$\mathbf{F}\bar{\mathbf{h}}\mathbf{F}^H = \text{diag}(\mathbf{F}\mathbf{h}) = \text{diag}(\mathbf{H}). \quad (3-22)$$

Then, the received signal \mathbf{Y} can be seen as the multiplication of the transmitted signal \mathbf{X} and the channel frequency response \mathbf{H}

$$\mathbf{Y} = \text{diag}(\mathbf{H})\mathbf{X} = \text{diag}(\mathbf{X})\mathbf{H} \quad (3-23)$$

3.2.1 LS and MMSE Channel Estimation

If the time domain channel vector $\mathbf{h} = [h(0), h(1), \dots, h(N-1)]^T$ is Gaussian and uncorrelated with the channel noise vector \mathbf{n} and set $\bar{\mathbf{X}} = \text{diag}(\mathbf{X})$, the MMSE estimate [15] of \mathbf{h} aims at minimizing $E \left[\left(\mathbf{Y} - \bar{\mathbf{X}}\mathbf{F}\mathbf{h} \right)^2 \right]$ becomes

$$\hat{\mathbf{h}}_{MMSE} = \mathbf{R}_{hY} \mathbf{R}_{YY}^{-1} \mathbf{Y}, \quad (3-24)$$

where

$$\mathbf{R}_{hY} = E\{\mathbf{h}\mathbf{Y}^H\} = \mathbf{R}_{hh} \mathbf{F}^H \bar{\mathbf{X}}^H \quad (3-25)$$

$$\mathbf{R}_{YY} = E\{\mathbf{Y}\mathbf{Y}^H\} = \bar{\mathbf{X}}\mathbf{F}\mathbf{R}_{hh}\mathbf{F}^H\bar{\mathbf{X}}^H + \sigma_n^2\mathbf{I}_n. \quad (3-26)$$

are the cross covariance matrix between \mathbf{h} and \mathbf{Y} and the auto-covariance matrix of \mathbf{Y} .

Further, \mathbf{R}_{hh} is the auto-covariance matrix of \mathbf{h} and $\sigma_n^2 = E\{|\mathbf{n}|^2\}$ denotes the noise variance. By using $(\mathbf{A} + \mathbf{BCD})^{-1} = \mathbf{A}^{-1} - \mathbf{A}^{-1}\mathbf{B}(\mathbf{DA}^{-1}\mathbf{B} + \mathbf{C}^{-1})^{-1}\mathbf{DA}^{-1}$ in [22], the MMSE estimate can be formulated as

$$\hat{\mathbf{H}}_{MMSE} = \mathbf{F}\hat{\mathbf{h}}_{MMSE} = \mathbf{F} \times \left(\mathbf{Q}_{MMSE} \mathbf{F}^H \bar{\mathbf{X}}^H \mathbf{Y} \right). \quad (3-27)$$

where

$$\mathbf{Q}_{MMSE} = \mathbf{R}_{hh} \left[\left(\mathbf{F}^H \bar{\mathbf{X}}^H \bar{\mathbf{X}} \mathbf{F} \right)^{-1} \sigma_n^2 + \mathbf{R}_{hh} \right]^{-1} \left(\mathbf{F}^H \bar{\mathbf{X}}^H \bar{\mathbf{X}} \mathbf{F} \right)^{-1}. \quad (3-28)$$

After some computation, the estimator can be computed as

$$\hat{\mathbf{H}}_{MMSE} = \mathbf{R}_{hh} (\mathbf{R}_{hh} + \sigma_n^2 (\mathbf{X}\mathbf{X}^H)^{-1})^{-1} \hat{\mathbf{H}}_{LS} \quad (3-29)$$

Besides, the LS estimator for \mathbf{h} which minimizes $(\mathbf{y} - \bar{\mathbf{X}}\mathbf{F}\mathbf{h})^H (\mathbf{y} - \bar{\mathbf{X}}\mathbf{F}\mathbf{h})$ can be represented as [22]:

$$\hat{\mathbf{H}}_{LS} = \mathbf{F}\mathbf{Q}_{LS}\mathbf{F}^H\bar{\mathbf{X}}^H\mathbf{Y}, \quad (3-30)$$

where

$$\mathbf{Q}_{LS} = (\mathbf{F}^H \bar{\mathbf{X}}^H \bar{\mathbf{X}} \mathbf{F})^{-1} \quad (3-31)$$

After some matrix computation, the estimator can be computed as

$$\begin{aligned} \hat{\mathbf{H}}_{LS} &= \begin{bmatrix} Y(0) & Y(1) & \dots & Y(N-1) \\ X(0) & X(1) & \dots & X(N-1) \end{bmatrix}^T \\ &= (\text{diag}(\mathbf{X}))^{-1} \mathbf{Y} \end{aligned} \quad (3-32)$$

For pilot-aided channel estimation using subcarrier allocation of IEEE 802.16 described in (2.2.2), only the pilot subcarriers are known at first, and thus the LS and MMSE schemes shall use the pilot information to estimate the channel frequency response at the pilot subcarriers first. The information contains two parameters, pilot magnitude $\mathbf{P} = [P_0, P_1, \dots, P_{N_p-1}]^T$ and pilot subcarrier index $\mathbf{f} = [f_0, f_1, \dots, f_{N_p-1}]^T$, where P_k stands for the magnitude of the k th pilot with subcarrier index f_k and N_p is the total number of pilot subcarriers. Thus, we can extract the received signal vector at the pilot subcarriers:

$$\mathbf{Y}_p = [Y(f_0), Y(f_1), \dots, Y(f_{N_p-1})]^T. \quad (3-33)$$

Then, the LS channel estimate in (3-32) can be modified as

$$\begin{aligned} \hat{\mathbf{H}}_{LS}^P &= \begin{bmatrix} Y(f_0) & Y(f_1) & \dots & Y(f_{N_p-1}) \\ P_0 & P_1 & \dots & P_{N_p-1} \end{bmatrix}^T \\ &= (\text{diag}(\mathbf{P}))^{-1} \mathbf{Y}_p \end{aligned} \quad (3-34)$$

and the MMSE channel estimation in (3-29) would be modified as

$$\hat{\mathbf{H}}_{MMSE}^P = \mathbf{R}_{hh} (\mathbf{R}_{hh} + \sigma_n^2 (\text{diag}(\mathbf{P}) \text{diag}(\mathbf{P})^H)^{-1})^{-1} \hat{\mathbf{H}}_{LS}^P \quad (3-35)$$

Afterwards, the interpolation method can be adopted to obtain the overall channel frequency response, which will be described in 3.2.2. The overall channel estimation approach are shown in Figure 3-5.

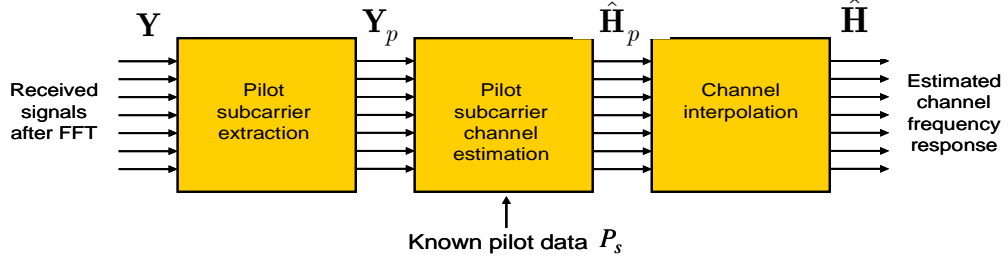


Figure 3-5: Pilot-aided channel estimation scheme

After the channel is estimated, a conventional equalization method using a one-tap equalizer can be employed to equalize the distorted received signals. Thus the decision output is

$$\hat{\mathbf{X}} = \text{dec} \left(\text{diag}(\hat{\mathbf{H}})^{-1} \mathbf{Y} \right) \quad (3-36)$$

3.2.2 Interpolation Techniques

After the estimation of the channel frequency response of pilot subcarriers, the channel response at the data subcarriers can be interpolated by adjacent pilot subcarriers. Several techniques described in [16] and [24] can be adopted to get the overall frequency response.

- **Linear interpolation:** Two successive pilot subcarriers are used to determine the channel response in between the pilot subcarriers. For data subcarrier k , $f_{j-1} < k \leq f_j$, the estimated channel response is given by

$$H_{\text{int erpl}}(k) = H^P(f_{j-1}) + \frac{k - f_{j-1}}{f_j - f_{j-1}} (H^P(f_j) - H^P(f_{j-1})). \quad (3-37)$$

- **Lagrange polynomial interpolation:** The linear interpolation can be further represented as

$$H_{\text{int erpl}}(k) = \frac{k - f_j}{f_{j-1} - f_j} H^P(f_{j-1}) + \frac{k - f_{j-1}}{f_j - f_{j-1}} H^P(f_j). \quad (3-38)$$

Thus, we can further increase the order of the interpolation function as the number of channel estimates at the pilot subcarriers used to estimate the channel response at one data subcarrier increases (not just the adjacent two pilot subcarriers)

$$H_{\text{interpl}}(k) = L_{j-N_u}(k)H^P(f_{j-N_u}) + L_{j-N_u+1}(k)H^P(f_{j-N_u+1}) + \cdots + L_{j+N_u-1}(k)H^P(f_{j+N_u-1}) \quad (3-39)$$

where

$$L_i(k) = \frac{(k - f_{j-N_u}) \cdots (k - f_{i-1})(k - f_{i+1}) \cdots (k - f_{j+N_u-1})}{(f_i - f_{j-N_u}) \cdots (f_i - f_{i-1})(f_i - f_{i+1}) \cdots (f_i - f_{j+N_u-1})} = \prod_{\substack{n=j-N_u \\ n \neq i}}^{j+N_u-1} \frac{k - f_n}{f_i - f_n} \quad (3-40)$$

and the k th data subcarrier estimate uses $2N_u$ adjacent pilot subcarrier estimates,

$$\{f_{j-N_u}, f_{j-N_u+1}, \cdots, f_{j+N_u-1}\}, \text{ for } f_{j-1} < k \leq f_j.$$

It is obvious that the linear interpolation uses the order of two of the Lagrange interpolation function and requires 2 multiplications for each desired subcarrier. If we extend the order to $2N_u$, the requirement in doing the Lagrange interpolation increases to $2N_u$ multiplications per subcarrier since the scaling term $L_i(k)$ in (3-40) remains constant for fixed subcarrier allocation.

3.2.3 Time Domain LS Channel Estimation

The frequency domain channel estimation methods described in 3.2.1 with interpolation techniques described in 3.2.2 would cause some problems. The interpolation methods may be sensitive to the noise and result in poor channel estimate if the SNR drops. Besides, for further reduction of the ICI effect, we have to

know the channel impulse response in time domain, which means the frequency domain channel estimate has to be transformed back to time domain. Besides the problem described above, the MMSE channel estimation has other drawback, including the requirement of the correlation matrix \mathbf{R}_{HH} , the noise variance δ_n^2 , and the large computation complexity incurred by matrix inversion.

In the following, a novel channel estimation technique proposed in [17] is adopted to meet the need for further ICI cancellation with moderate complexity, which can be regarded as the time domain LS channel estimation. First of all, the entire frequency response for the received signal \mathbf{Y} can be represented as

$$\begin{aligned}
 \mathbf{Y} &= \begin{bmatrix} X(0) & 0 & \dots & 0 \\ 0 & X(1) & \dots & 0 \\ \vdots & \dots & \ddots & \vdots \\ 0 & \dots & 0 & X(N-1) \end{bmatrix} \\
 &\times \begin{bmatrix} e^{-j2\pi \frac{0*0}{N}} & \dots & e^{-j2\pi \frac{0*(N-1)}{N}} \\ \vdots & \ddots & \vdots \\ e^{-j2\pi \frac{(N-1)*0}{N}} & \dots & e^{-j2\pi \frac{(N-1)*(N-1)}{N}} \end{bmatrix} \begin{bmatrix} h_0 \\ \vdots \\ h_G \\ \vdots \\ h_{N-1} \end{bmatrix}. \quad (3-41) \\
 &= \mathit{diag}(\mathbf{X})\mathbf{F}\mathbf{h}
 \end{aligned}$$

For pilot-based channel estimation, pilot information is known first. The information contains two parameters, pilot magnitude vector $\mathbf{P} = [P_0, P_1, \dots, P_{p-1}]^T$ and pilot subcarrier index vector $\mathbf{f} = [f_0, f_1, \dots, f_{p-1}]^T$, where P_k stands for the magnitude of the k th pilot with subcarrier index f_k and p is the total number of the pilot subcarriers. For the channel impulse response vector \mathbf{h} , let $\mathbf{g} = [g_0, g_1, \dots, g_{L-1}]^T$ be the non-zero channel tap gain and τ_i the

corresponding path delay for g_i , where L denotes the total number of paths in discrete samples. Specifically, \mathbf{h} can be divided into two groups:

$$\begin{cases} h_i = g_j & \text{for } i = \tau_j \\ h_i = 0 & \text{for } i \neq \tau_j \end{cases} \quad (3-42)$$

It is obvious that \mathbf{g} is the non-zero group of the entire impulse response. Therefore,

(3-41) can be modified to show the response of the received pilot signal:

$$\begin{aligned} \mathbf{Y}_p &= [Y(f_0), Y(f_1), \dots, Y(f_{p-1})]^T \\ &= \mathbf{X}_p \mathbf{F}_{LP} \mathbf{g} \end{aligned} \quad (3-43)$$

where

$$\begin{aligned} \mathbf{X}_p &= \begin{bmatrix} P_0 & 0 & \dots & 0 \\ 0 & P_1 & \dots & 0 \\ \vdots & \dots & \ddots & \vdots \\ 0 & \dots & 0 & P_{p-1} \end{bmatrix} = \text{diag}(\mathbf{P}) \\ \mathbf{F}_{LP} &= \begin{bmatrix} e^{-j2\pi \frac{f_0^* \tau_0}{N}} & e^{-j2\pi \frac{f_0^* \tau_1}{N}} & \dots & e^{-j2\pi \frac{f_0^* \tau_{L-1}}{N}} \\ e^{-j2\pi \frac{f_1^* \tau_0}{N}} & e^{-j2\pi \frac{f_1^* \tau_1}{N}} & \dots & e^{-j2\pi \frac{f_1^* \tau_{L-1}}{N}} \\ \vdots & \dots & \ddots & \vdots \\ e^{-j2\pi \frac{f_{p-1}^* \tau_0}{N}} & \dots & e^{-j2\pi \frac{f_{p-1}^* \tau_{L-2}}{N}} & e^{-j2\pi \frac{f_{p-1}^* \tau_{L-1}}{N}} \end{bmatrix} \end{aligned} \quad (3-44)$$

The matrix \mathbf{F}_{LP} can be viewed as the modified DFT matrix which only calculates the non-zero part of the impulse response and transmitted pilot signal. Then, a least square estimate of the impulse response of the wireless channel may be obtained to minimize $(\mathbf{Y}_p - \mathbf{X}_p \mathbf{F}_{LP} \mathbf{g})^H (\mathbf{Y}_p - \mathbf{X}_p \mathbf{F}_{LP} \mathbf{g})$. The time domain LS estimate can be derived based on the initial frequency response estimate as

$$\hat{\mathbf{g}}_{T-LS} = \left(\mathbf{F}_{LP}^H \mathbf{X}_p^H \mathbf{X}_p \mathbf{F}_{LP} \right)^{-1} \times \mathbf{F}_{LP}^H \mathbf{X}_p^H \mathbf{Y}_p \quad (3-46)$$

At last, an enhanced estimate of the frequency response of the wireless channel can be derived for a group of data subcarriers based on the impulse response estimate can be

obtained as

$$\hat{\mathbf{H}}_{T-LS} = \mathbf{F}\hat{\mathbf{h}}_{T-LS}, \quad (3-47)$$

where

$$\hat{h}_{T-LS}(i) = \begin{cases} \hat{g}_{T-LS}(i) & \text{for } i = \tau_j \\ 0 & \text{for } i \neq \tau_j \end{cases}. \quad (3-48)$$

Since data are transmitted in only a few subcarriers for one user in the OFDMA system, the DFT matrix, \mathbf{F} , can be modified to produce only the required subcarriers to reduce the complexity. After the channel is estimated, a conventional equalization method using a one-tap equalizer can be employed to equalize the distorted received signals in (3-36).

Since the pilot information is fixed and known to the receiver, \mathbf{X}_p is a constant vector. That means it can be constructed first to prevent from the computation load in performing this channel estimation. Furthermore, the multipath number L and delay vector τ have to be estimated first. From (3-46), the inversion of the $(L \times L)$ matrix may consume much of the processing time. But if there are only few multipaths, which means that L is small, the complexity in doing this inversion can be low. Furthermore, if the multipath number and delay do not change, \mathbf{F}_{LP} is a constant matrix and thus its inverse is also a constant matrix in the channel estimation process. For the final FFT to transform the impulse estimate into the channel frequency response estimate, the nature of OFDMA reduces much of the load because only a limited part of subcarriers are involved.

Figure 3-6 shows the performance of the frequency domain and time domain LS channel estimation. The frequency domain LS channel estimation uses linear interpolation and Lagrange interpolation of order four and six for data subcarriers. It

can be seen that the time domain LS channel estimation always has better performance. It is because that the frequency domain LS estimation will suffer from the inaccuracy due to the interpolation when the channel has large path delay.

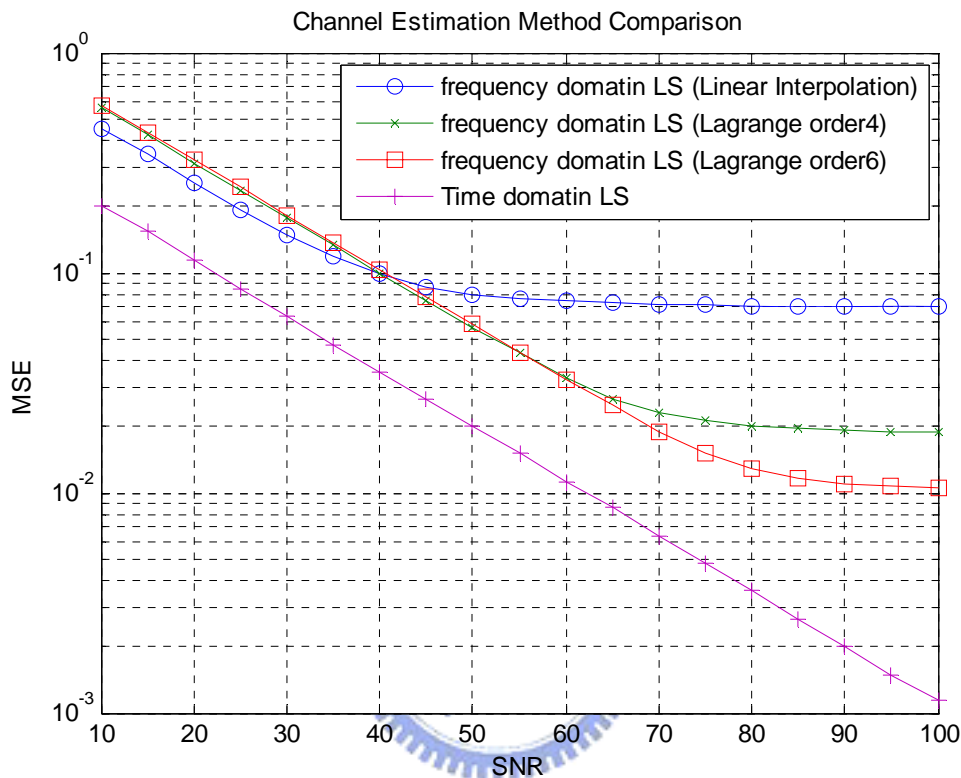


Figure 3-6: Comparison of two channel estimation methods

3.3 Summary

In this chapter, channel models for different environment are described in 3.1 first. Then, system description for pilot-aided OFDM is shown and several channel estimation approaches to equalize the channel effect are introduced. From the simulation, the time domain LS channel estimation is shown to have more precise estimate than that of frequency domain LS channel estimation. The channel tap gain estimate can be used to further mitigate the ICI induced by the time varying channel, which will be the main topic in the next chapter.

Chapter 4

ICI Mitigation for Mobile WiMAX Systems

For mobile applications channel time-variations in one OFDM symbol introduce intercarrier-interference (ICI) which degrades the performance. Therefore, to have an acceptable reception quality, there is a need for ICI mitigation within one OFDM symbol. In this chapter, piece-wise linear model is used to model the variation of the time channel response. Taylor series expansion can be used to further track the channel varying nature using higher derivatives of the channel amplitude. Afterwards, channel matrix can be constructed to specify the effect each subcarrier has upon the others. By canceling the effect caused by each carrier, ICI phenomenon can be resolved and thus improve the performance. Furthermore, an iterative PIC algorithm can be designed to mitigate the ICI effects

4.1 Channel Analysis with ICI Induced by Mobility

In conventional channel estimation assumption, channel is assumed to be quasi-stationary, which means that multipath gain is constant in each symbol period. But for the fast moving mobile channel, this assumption neglects all the interferences the varying channel may cause.

The time varying channel output can be expressed as

$$y_i = \sum_{k=0}^G \tilde{h}_k^{(i)} x_{((i-k))_N} + w_i \quad 0 \leq i \leq N-1, \quad (4-1)$$

where $\tilde{h}_k^{(i)}$ indicates the k th channel tap gain in the i th time sample with the assumption that the largest channel tap delay is not larger than the guard interval G .

For time invariant channel, $\tilde{h}_k^{(i)}$ can be viewed as a constant from $i = 0$ to $i = N - 1$. Express (4-1) in Matrix form:

$$\mathbf{y} = \tilde{\mathbf{h}}\mathbf{F}^H \mathbf{X} + \mathbf{w}. \quad (4-2)$$

It can be easily shown that

$$\tilde{\mathbf{h}} = \begin{bmatrix} \tilde{h}_0^{(0)} & \mathbf{0} & \tilde{h}_G^{(0)} & \dots & \tilde{h}_1^{(0)} \\ \tilde{h}_1^{(1)} & \tilde{h}_0^{(1)} & \mathbf{0} & \tilde{h}_G^{(1)} & \dots \\ \vdots & \vdots & \ddots & \dots & \dots \\ \mathbf{0} & \tilde{h}_G^{(N-1)} & \dots & \tilde{h}_0^{(N-1)} & \mathbf{0} \end{bmatrix}. \quad (4-3)$$

In time-invariant system, $\tilde{h}_k^{(i)}$ is constant for each k and thus (4-3) can be shown as a circulant matrix.

After the FFT computation, the frequency domain received signal can be expressed as follows:

$$Y_i = \tilde{H}_{i,i}X_i + \sum_{d=0, d \neq i}^{N-1} \tilde{H}_{i,d}X_d + W_i \quad 0 \leq i \leq N-1, \quad (4-4)$$

where

$$F_m(i, d) = \sum_{u=0}^{N-1} \tilde{h}_m^{(u)} e^{-j \frac{2\pi u((d-i))}{N}} \quad 0 \leq m \leq G \quad (4-5)$$

$$\tilde{H}_{i,d} = \frac{1}{N} \sum_{m=0}^G F_m(i, d) e^{-j \frac{2\pi m d}{N}} \quad 0 \leq i, d \leq N-1. \quad (4-6)$$

This is equivalent to two FFT operations: first the time channel response is transformed with respect to the time index and the distance between data carrier and interference carrier, and then the resulting value is transformed with respect to the path delay and the data subcarrier index.

The frequency domain received data \mathbf{Y} in matrix form is shown below:

$$\begin{bmatrix} Y_0 \\ \vdots \\ \vdots \\ Y_{N-1} \end{bmatrix} = \begin{bmatrix} \tilde{H}_{0,0} & \tilde{H}_{0,1} & \cdots & \tilde{H}_{0,N-1} \\ \tilde{H}_{1,0} & \ddots & \cdots & \tilde{H}_{1,N-1} \\ \vdots & \cdots & \cdots & \vdots \\ \tilde{H}_{N-1,0} & \cdots & \tilde{H}_{N-1,N-2} & \tilde{H}_{N-1,N-1} \end{bmatrix} \times \begin{bmatrix} X_0 \\ \vdots \\ \vdots \\ X_{N-1} \end{bmatrix} + \begin{bmatrix} W_0 \\ \vdots \\ \vdots \\ W_{N-1} \end{bmatrix} \quad (4-7)$$

$$= \tilde{\mathbf{H}}\mathbf{X} + \mathbf{W}$$

It can be easily shown that $\tilde{\mathbf{H}}$ is not a diagonal matrix anymore, which means that each received data subcarrier not only depends on the same transmitted data subcarrier but also all the other subcarriers. $\tilde{H}_{i,d}$ is the scaling term from d th transmitted subcarrier to the i th received subcarrier. For $i \neq d$, $\tilde{H}_{i,d}X_d$ is the ICI term to Y_i . To see the characteristics of the matrix $\tilde{\mathbf{H}}$, Figure 4-1 plots the coupling channel matrix in three dimensions.

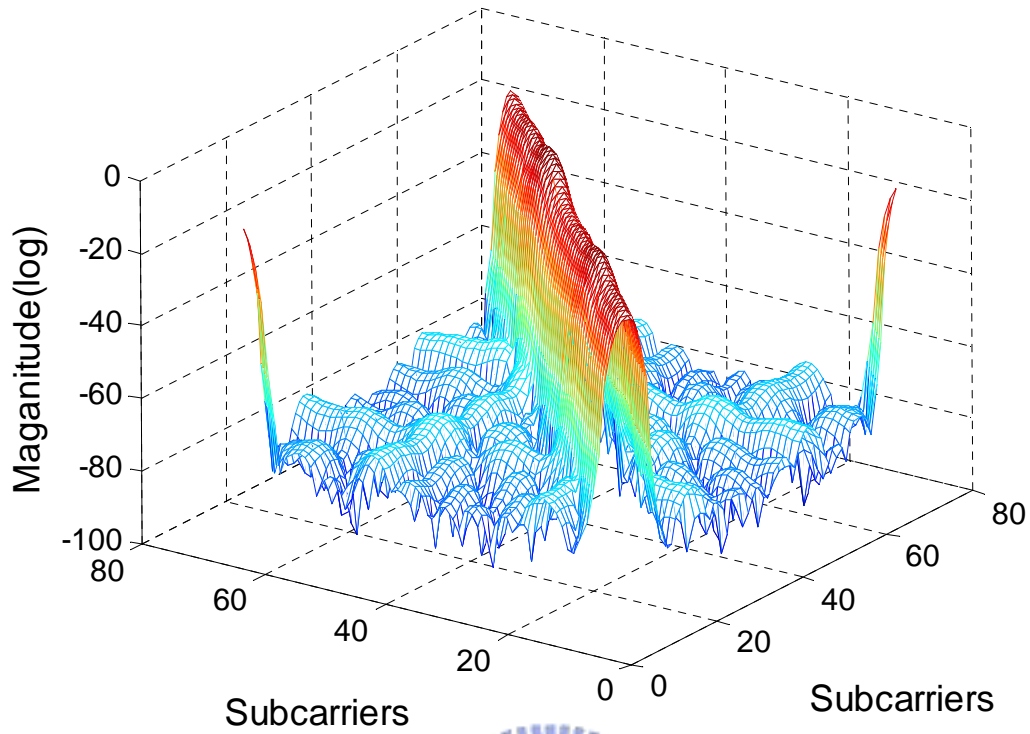


Figure 4-1: Plot of channel matrix



Furthermore,

$$\tilde{h}_m^{ave} = (1/N) \sum_{u=0}^{N-1} \tilde{h}_m^u \quad (4-8)$$

$$\tilde{H}_{i,i} = \sum_{m=0}^G \tilde{h}_m^{ave} e^{-j \frac{2\pi m i}{N}}, \quad (4-9)$$

where \tilde{h}_m^{ave} is the average of the m th channel tap over the time duration of $0 \leq u \leq N - 1$. In the time-invariant system, $\tilde{\mathbf{H}}$ becomes a diagonal matrix (using the nature of transforming a circulant matrix to frequency domain), and the one-tap equalizer is sufficient for compensating the channel effect.

The problem to be discussed now is how to derive the ICI term depending on the channel estimation result developed in Chapter 3.

4.2 ICI Modeling

4.2.1 Piece-wise Linear Model

By using the time domain LS channel estimate, we can obtain the entire impulse response estimate in each symbol period. Since each channel tap gain varies within a symbol, the quasi static assumption that it is constant in a symbol period is unsatisfactory as the maximum Doppler shift, f_d , increases.

In this section, linear approximation is applied to derive the frequency domain relationship developed in 4.1. To perform the linearization, we have to know how to model the channel at one time instant in the symbol. For the k th channel tap,

$E\left(\left|\tilde{h}_k^{ave} - \tilde{h}_k^{(s)}\right|^2\right)$ is minimized for $s = \left(\frac{N}{2} - 1\right)$, where \hat{h}_k^{ave} is defined in (4.8).

Therefore, we approximate $\tilde{h}_k^{(N/2-1)}$ with the estimate of \tilde{h}_k^{ave} :

$$\hat{h}_k^{(N/2-1)} = \hat{h}_k^{ave}. \quad (4-10)$$

Let α_m denotes the slope of the m th channel tap gain at $\hat{h}_{\tau_m}^{(N/2-1)}$ in the current OFDM symbol and τ_m is the delay of this path. Using the piece-wise linear model which approximates channel time-variations with a constant slope over the time duration, $\tilde{h}_{\tau_m}^i$ can be approximated as

$$\tilde{h}_{\tau_m}^i \approx \hat{h}_{\tau_m}^{(N/2-1)} + \left(i + 1 - \frac{N}{2}\right) \times \alpha_m \quad (4-11)$$

$$0 \leq i \leq N - 1$$

Figure 4-2 illustrates the piece-wise linear model, where solid curve stands for real or imaginary part of a channel path and dashed line stands for piece-wise linear model.

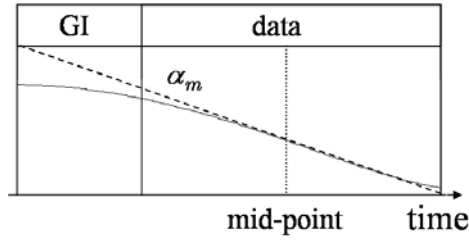


Figure 4-2: Piece-wise linear model

Using the time domain LS channel estimate developed in Chapter 3, the entire impulse response is estimated in each symbol period, which was shown in [6] to be close to $\hat{h}_{\tau_m}^{(N/2-1)}$

$$\hat{h}_{T-LS}(\tau_m) \approx \hat{h}_{\tau_m}^{(N/2-1)} \quad m = 0 \sim L-1 \quad (4-12)$$

Then, using the neighboring symbols, we can extend (4-11) by using two slopes to model the channel variation for each symbol:

$$\tilde{h}_{\tau_m}^i \approx \begin{cases} i = 0 \sim \frac{N}{2} - 1: & \hat{h}_{T-LS}(\tau_m) + (i+1 - \frac{N}{2}) \times \alpha_m^0 \\ i = \frac{N}{2} \sim N-1: & \hat{h}_{T-LS}(\tau_m) + (i+1 - \frac{N}{2}) \times \alpha_m^1 \end{cases} \quad (4-13)$$

The figure representation is shown in Figure 4-3, where solid curve stands for real or imaginary part of a channel path and dashed line stands for piece-wise linear model using the previous and the next symbols.

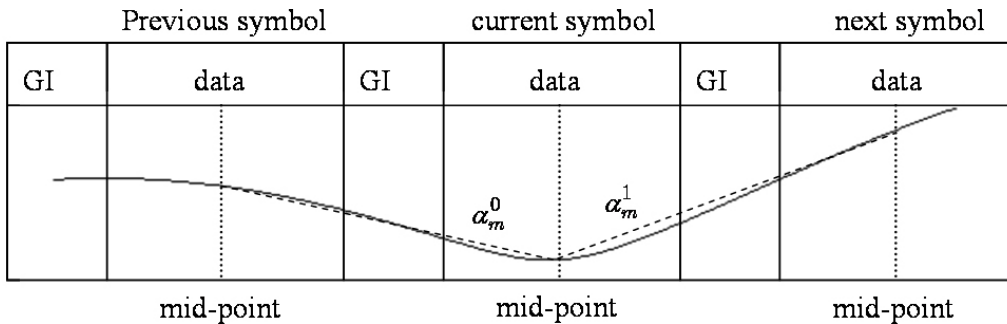


Figure 4-3: Piece-wise linear model using symbols nearby

Therefore, (4.5) can be simplified as

$$\begin{aligned}
F_{\tau_m}(i, d) &= \sum_{u=0}^{N-1} \tilde{h}_{\tau_m}^{(u)} e^{-j \frac{2\pi u((d-i))_N}{N}} \\
&= \sum_{u=0}^{N-1} \hat{h}_{T-LS}(\tau_m) \times e^{-j \frac{2\pi u((d-i))_N}{N}} \\
&\quad + \alpha_m^0 \times \sum_{u=0}^{\frac{N}{2}-1} \left(u + 1 - \frac{N}{2} \right) \times e^{-j \frac{2\pi u((d-i))_N}{N}} \\
&\quad + \alpha_m^1 \times \sum_{u=\frac{N}{2}}^{N-1} \left(u + 1 - \frac{N}{2} \right) \times e^{-j \frac{2\pi u((d-i))_N}{N}}.
\end{aligned} \tag{4-14}$$

Set

$$c_m^0(d-i) = \sum_{u=0}^{\frac{N}{2}-1} \left(u + 1 - \frac{N}{2} \right) \times e^{-j \frac{2\pi u((d-i))_N}{N}} \tag{4-15}$$

$$c_m^1(d-i) = \sum_{u=\frac{N}{2}}^{N-1} \left(u + 1 - \frac{N}{2} \right) \times e^{-j \frac{2\pi u((d-i))_N}{N}} \tag{4-16}$$

$$\mathbf{c}_m^0 = \left[c_m^0(0) \quad c_m^0(1) \quad \cdots \quad c_m^0(N-1) \right]^T \tag{4-17}$$

$$\mathbf{c}_m^1 = \left[c_m^1(0) \quad c_m^1(1) \quad \cdots \quad c_m^1(N-1) \right]^T \tag{4-18}$$

It is obvious that \mathbf{c}_m^0 and \mathbf{c}_m^1 are fixed vectors; that is, they act as system constants which adapt neither to the data nor to the channel. No computation is needed here while the ICI mitigation mechanism is ongoing.

From (4-6) and (4-14), the frequency domain channel matrix $\tilde{\mathbf{H}}$ can be modeled as:

$$\begin{aligned}
\tilde{H}_{i,d} &= \frac{1}{N} \sum_{m=0}^{L-1} F_{\tau_m}(i,d) e^{-\frac{2\pi\tau_m d}{N}} \quad 0 \leq i, d \leq N-1 \\
&= \begin{cases} \sum_{m=0}^{L-1} \left(\hat{h}_{T-LS}(\tau_m) + \frac{1}{N} \left(\alpha_m^0 c_m^0(0) + \alpha_m^1 c_m^1(0) \right) \right) \times e^{-j\frac{2\pi\tau_m d}{N}}, & i = d \\ \frac{1}{N} \sum_{m=0}^{L-1} \left(\alpha_m^0 c_m^0(d-i) + \alpha_m^1 c_m^1(d-i) \right) \times e^{-j\frac{2\pi\tau_m d}{N}}, & i \neq d \end{cases} \quad (4-19)
\end{aligned}$$

Then, the received signal at the i th subcarrier can be constructed as the combination of the channel response of the transmitted signal at the i th carrier and the ICI term from other carriers plus noise.

$$\begin{aligned}
Y_i &= \tilde{H}_{i,i} X_i + \sum_{d=0, d \neq i}^{N-1} \tilde{H}_{i,d} X_d + W_i \quad 0 \leq i \leq N-1 \\
&= \tilde{H}_{i,i} X_i \\
&\quad + \sum_{d=0, d \neq i}^{N-1} \left[\frac{1}{N} \sum_{m=0}^{L-1} \left(\alpha_m^0 \times c_m^0(d-i) + \alpha_m^1 \times c_m^1(d-i) \right) \times e^{-j\frac{2\pi\tau_m d}{N}} \right] \times X_d + W_i
\end{aligned} \quad (4-20)$$

The second term in (4-20) can be viewed as the ICI of this subcarrier, which is the combination of all the interferences from the other subcarriers.

$$ICI_i = \sum_{d=0, d \neq i}^{N-1} \left[\frac{1}{N} \sum_{m=0}^{L-1} \left(\alpha_m^0 \times c_m^0(d-i) + \alpha_m^1 \times c_m^1(d-i) \right) \times e^{-j\frac{2\pi\tau_m d}{N}} \right] \times X_d \quad (4-21)$$

In summary, the time domain LS channel estimate would give the impulse response estimate at $t = N/2 - 1$ for each path in each symbols. Then, for the symbol we wish to mitigate the ICI effect, the slopes from the current symbol to the previous and the next symbol can be gained. The ICI term for certain subcarrier can then be generated as the combination of all the interferences from the other subcarriers. The better we have knowledge about X_d , the better interference can be canceled (will be discussed later).

4.2.2 Taylor Series Modeling

From 4.2.1, the time-varying channel response using piece-wise linear model has been developed. For rapid fading channel, piece-wise linear approximation may not be adequate to model the channel variation.

For the time-varying function $h(t)$, we can represent it as the combination of each derivative of the function by using the Taylor Series:

$$h(t) = h(a) + h'(a)(t-a) + \dots + \frac{h^{(p)}(a)}{p!}(t-a)^p + \dots \quad (4-22)$$

Then, the channel model can be modeled as a function of u around $u = N/2$:

$$\begin{aligned} \tilde{h}_i^{(u)} &= \beta_i^0 + \left(u - \frac{N}{2}\right) \beta_i^1 + \frac{\left(u - \frac{N}{2}\right)^2}{2!} \beta_i^2 + \dots + \frac{\left(u - \frac{N}{2}\right)^p}{p!} \beta_i^p + \dots \\ &= \sum_{p=0}^{\infty} \beta_i^p \frac{\left(u - \frac{N}{2}\right)^p}{p!} \end{aligned} \quad (4-23)$$

where $\beta_i^{(p)}$ indicates the p th derivative term of $h_i(t)$ at $t = NT/2$:

$$\beta_i^{(p)} = \left. \left(\frac{d^{(p)} h_i(t)}{d^{(p)} t} \right) \right|_{t=NT/2} . \quad (4-24)$$

Following (4-7), the received signal in frequency domain can be further represented as the combination of each derivative term of the channel tap gain:

$$Y_i = \sum_{d=0}^{N-1} \left(\frac{1}{N} \sum_{m=0}^{L-1} \left(\sum_{u=0}^{N-1} \tilde{h}_{\tau_m}^{(u)} \times e^{-j2\pi \frac{u((d-i))_N}{N}} \right) \times e^{-j2\pi \frac{\tau_m d}{N}} \right) X_d + W_i . \quad (4-25)$$

To adopt a matrix representation, we define

$$H_k^{(p)} = \sum_{m=0}^{L-1} \beta_{\tau_m}^{(p)} e^{-j2\pi \frac{\tau_m k}{N}} , \quad (4-26)$$

where $k = 0, 1, \dots, N-1$ and the vector form of the p th derivative can be collected

as

$$\mathbf{H}^{(p)} = [H_0^{(p)}, H_1^{(p)}, H_2^{(p)}, \dots, H_{N-1}^{(p)}]. \quad (4-27)$$

Then, (4-25) can be written as the matrix form

$$\mathbf{Y} = \left(\sum_{p=0}^{\infty} \Xi^{(p)} \text{diag} \{ \mathbf{H}^{(p)} \} \right) \mathbf{X} + \mathbf{W}, \quad (4-28)$$

where

$$[\Xi^{(p)}]_{m,k} = \frac{1}{N} \sum_{u=0}^{N-1} \frac{\left(u - \frac{N}{2}\right)^p}{p!} e^{-2\pi j \frac{u((m-k))_N}{N}}. \quad (4-29)$$

For (4-29), $\Xi^{(p)}$ is a fixed matrix which can be viewed as a system constant and constructed before processing to reduce the computation load.

It can be seen from (4-26) and (4-28) that if we can derive the p th derivative $\beta_i^{(p)}$ of the channel time variation at $t = NT/2$ for each path, then the ICI induced by this derivative term of the channel can be constructed and thus canceled. For the estimation of the derivative vector $\{ \mathbf{H}^{(p)} \}$, some mechanism can be introduced to estimate certain derivative term. From 4.2.1, first order derivative term ($p = 1$) is used to mitigate the ICI. For more derivative terms, polynomial interpolation [16] can be adopted. For the varying function

$$\hat{x}(t) = a_0 + a_1 t + a_2 t^2 + \dots + a_N t^N, \quad (4-30)$$

each derivative term can be found by using the polynomial interpolation:

$$\begin{bmatrix} a_0 \\ a_1 \\ a_2 \\ \vdots \\ a_N \end{bmatrix} = \begin{bmatrix} 1 & t_0 & t_0^2 & \dots & t_0^N \\ 1 & t_1 & t_1^2 & \dots & t_1^N \\ 1 & t_2 & t_2^2 & \dots & t_2^N \\ \vdots & \vdots & \vdots & \ddots & \vdots \\ 1 & t_N & t_N^2 & \dots & t_N^N \end{bmatrix}^{-1} \begin{bmatrix} x(t_0) \\ x(t_1) \\ x(t_2) \\ \vdots \\ x(t_N) \end{bmatrix}. \quad (4-31)$$

From (4-23) and (4-31), the first and second derivative terms can be obtained from the

previous and the next symbol channel estimate:

$$\begin{bmatrix} \beta_i^0 \\ \beta_i^1 \\ \frac{\beta_i^2}{2} \end{bmatrix} = \begin{bmatrix} 1 & -t & (-t)^2 \\ 1 & 0 & 0 \\ 1 & t & (t)^2 \end{bmatrix}^{-1} \begin{bmatrix} \hat{h}_i^{(N/2-1)}(symbol_{-1}) \\ \hat{h}_i^{(N/2-1)}(symbol_0) \\ \hat{h}_i^{(N/2-1)}(symbol_1) \end{bmatrix}, \quad (4-32)$$

where $t = CP_len + fft_len$ is the distance between two mid points of the two nearby symbols. The inverse matrix in (4-32) can be constructed in advance without adding load to the system.

Figure 4-4 shows the mean square error of three kinds of approximation to a varying channel. LS approximation means that the varying channel is approximated as constant in one symbol period. First order approximation stands for the application of the piece-wise linear method, and second order approximation stands for the application of the polynomial interpolation method.

Figure 4-5 shows the magnitude of three kinds of approximation to a varying channel. We can see that second order approximation best fit the channel variation from both Figure 4-4 and Figure 4-5

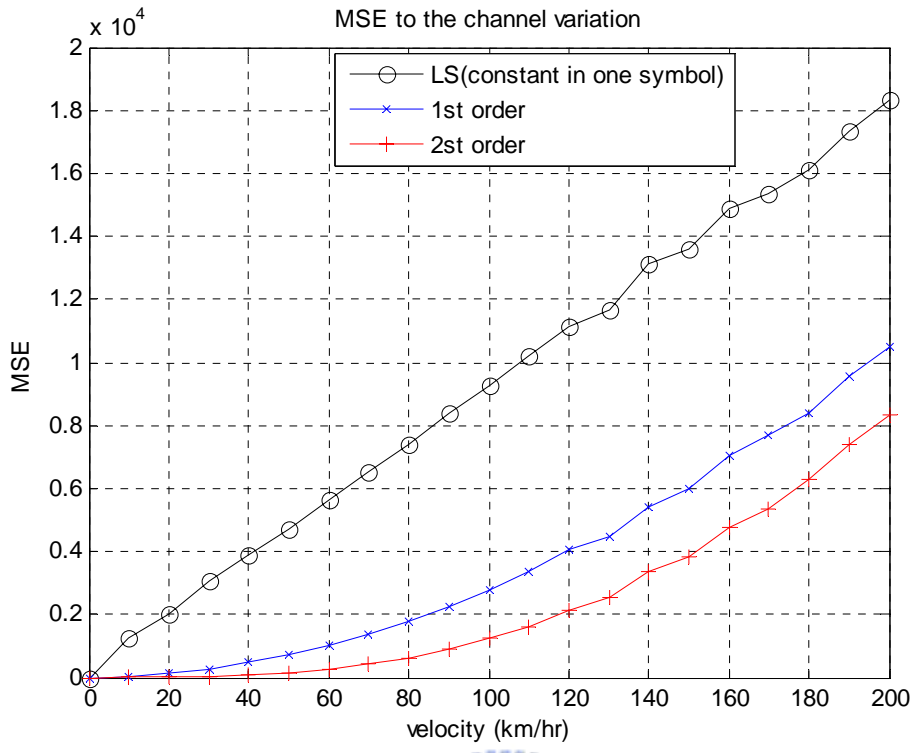


Figure 4-4: Mean square error of different approximations to the varying channel

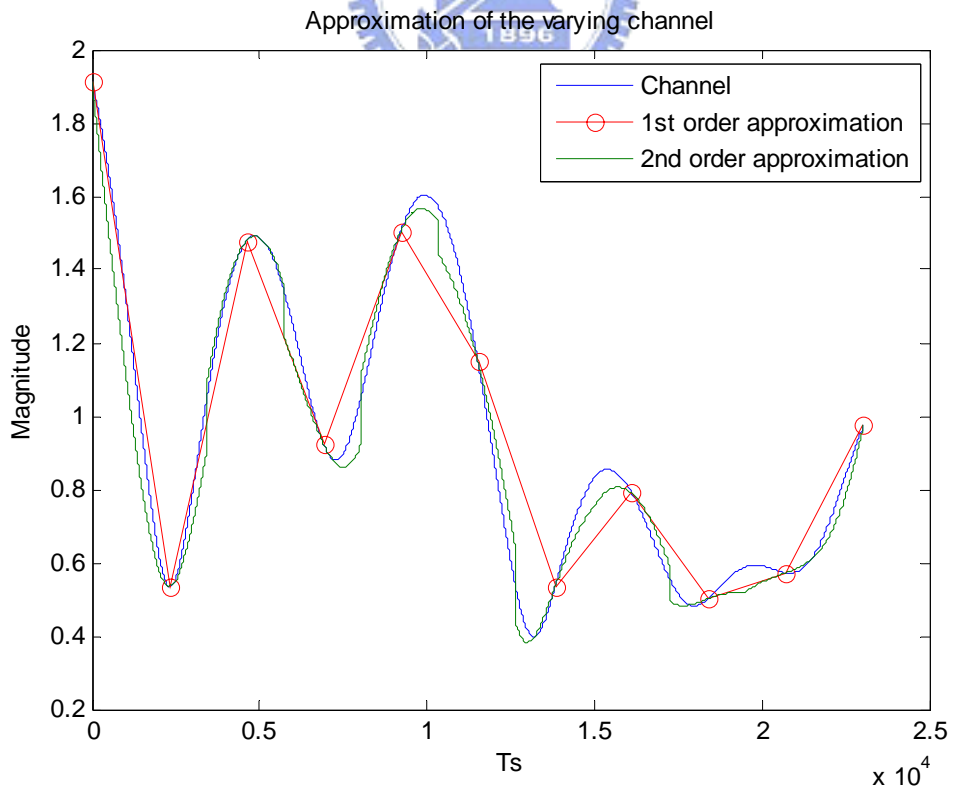


Figure 4-5: Magnitude of different approximations to the varying channel

From (4-25), the ICI vector can be modeled as

$$\mathbf{ICI} = \begin{bmatrix} ICI_0 \\ \vdots \\ ICI_{N-1} \end{bmatrix} = \left(\sum_{p=1}^2 \Xi^{(p)} \text{diag}\{\mathbf{H}^{(p)}\} \right) \mathbf{X} \quad (4-33)$$

To summarize, the time domain LS channel estimate would estimate the channel tap gain at $t = N/2 - 1$ for each path in each symbol. Then, for the symbol we want to mitigate the ICI effect, the first and second derivatives with the previous and the next symbol can be gained by applying the polynomial interpolation method and thus $\mathbf{H}^{(0)}$ and $\mathbf{H}^{(1)}$ defined in (4-28). The interference can be canceled for good data estimate $\hat{\mathbf{X}}$.

4.3 Combined Channel Estimation and ICI Mitigation

4.3.1 Data Detection Techniques

The two ICI mitigation methods described in 4.2.1 and 4.2.2, Piecewise Linear and Taylor Approximate, require the accurate estimate of the transmitted signal $\hat{\mathbf{X}}$ to effectively cancel the ICI, which are shown in (4-21) and (4-33).

The signal $\hat{\mathbf{X}}$ consists of two kind of information among the subcarriers: pilot information and data information. Since the pilot information of all pilot subcarriers is known, the interference caused by pilot can be perfectly removed. For the data information, first the received signal shall pass through the zero-forcing (ZF) equalizer to roughly compensate the channel effect:

$$\hat{X}_d = \frac{Y_d}{H_{d,d}}. \quad (4-34)$$

Then, nearest point data detection method can be applied to approximate the data subcarriers beside pilot, which is illustrated in Figure 4-6. The circle stands for the

correct signal constellation, and the star stands for the received signal after zero-forcing equalizer. After the nearest point data detection method, the star will be moved to the nearest circle in the knowing that the signal plus noise and interference occurs to be most likely the nearest correct signal constellation.

It is clear that the more accurate the data detection is, the more ICI can be precisely cancelled. There are still other data detection schemes. For example, data detection can be performed by de-interleaving and decoding first and then re-encoding and re-interleaving according to the IEEE 802.16-2005 standard. The detection is more robust at the cost of large computation complexity and delay.

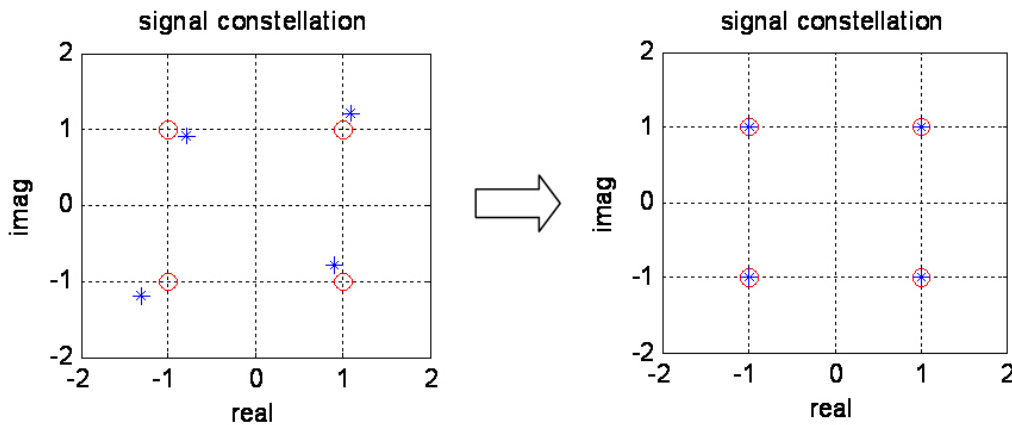


Figure 4-6: Nearest point data detection method

4.3.2 PIC Equalizer

After data is detected, the PIC equalizer proposed in [10] can then be used to subtract the ICI term from \mathbf{Y} according to (4-21) and (4-33). As seen in Figure 4-7, the PIC equalizer consists of two stages. In order to subtract the ICI term from the symbol Y_i , we need to know all the symbols $X_j (j \neq i)$ of ICI term. However, we cannot get prior knowledge of the symbols of the ICI term. In order to obtain the

accurate symbols of the ICI term, the received signal vector is fed to the one-tap equalizer and data detection filter in the first stage. Then the initial decision is fed to the ICI cancellation filter to cancel the ICI term in the second stage.

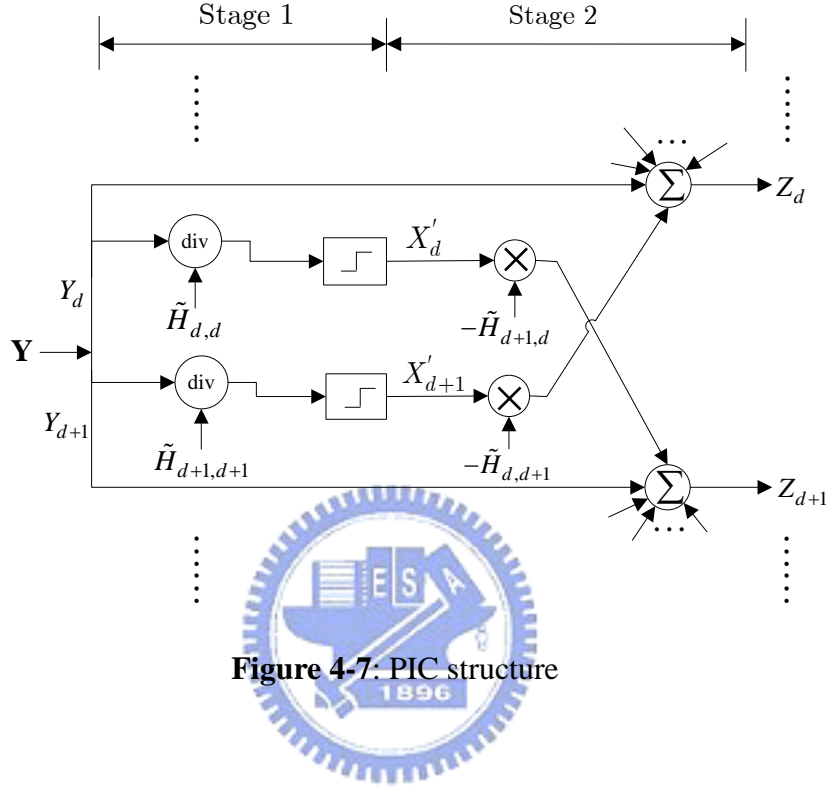


Figure 4-7: PIC structure

A. First Stage of the PIC Equalizer:

In the first stage of the PIC equalizer, the received signal vector, $[Y_0, Y_1, \dots, Y_{N-1}]$, is first fed to the one-tap equalizer. This is the conventional approach to equalizing the distorted signals:

$$\hat{X}_d = \frac{Y_d}{\tilde{H}_{d,d}} = X_d + \sum_{i=0, i \neq d}^{N-1} \frac{H_{d,i} X_i}{\tilde{H}_{d,d}} + \frac{W_d}{\tilde{H}_{d,d}}. \quad (4-35)$$

After the one-tap equalizer compensates for the multiplicative distortion, the output signal \hat{X}_d contains only the desired signal, ICI, and noise. Then, the initial decision

can be made as \hat{X}'_d , given by

$$\hat{X}'_d = dec(\hat{X}_d), \quad (4-36)$$

where the decision function denotes the data detection method described in 4.3.1.

B. Second Stage of the PIC Equalizer:

In the second stage, the initial decisions are utilized to cancel the ICI effect. For the p th desired subcarrier, the initial decisions \hat{X}_d' , for $d = 1, \dots, p-1, p+1, \dots, N$, are multiplied by the channel response $\hat{H}_{p,d}$ to get the interference estimate from the d th subcarrier to the p th desired subcarrier. The received signal Y_p can eliminate the ICI from all the estimated interference and thus gain the clean signal Z_p without ICI:

$$Z_p = Y_p - \sum_{d=0, d \neq p}^{N-1} H_{p,d} X_d' . \quad (4-37)$$

The system structure shown in Figure 4-8 can be used to perform the entire ICI cancellation mechanism, including the channel estimation, one-tap equalizer, data detection, ICI generator, and the ICI canceller. It is obvious that the (3), (4), (5), and (6) blocks in the figure correspond to the PIC structure in Figure 4-7. The received signal vector \mathbf{Y} first passes through the channel estimator to get the channel estimate which can further generate the ICI term. After the ICI is estimated, the received signal vector \mathbf{Y} can eliminate the ICI effect in parallel fashion. The clean signal vector \mathbf{Z} is produced and can be fed back to replace the channel estimator input \mathbf{Y} and therefore gain better channel estimate and detected data. These better estimates can promise a cleaner \mathbf{Z} free from more ICI. This iterative scheme can be terminated by setting the number of iteration N_I . The complete iterative procedure can be summarized in Table 4-1.

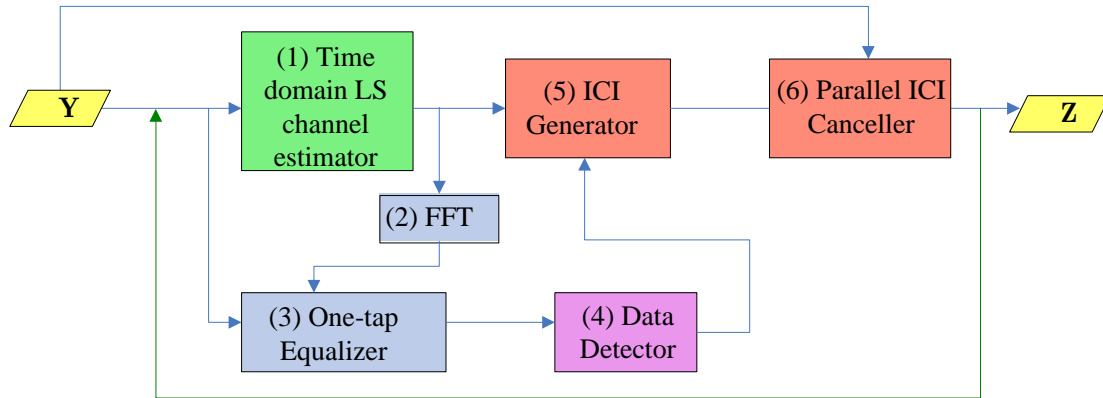


Figure 4-8: System Structure

Table 4-1: Iterative ICI cancellation procedure

Step	Command
1	Perform (1) Time domain LS channel estimation to get the time domain channel estimate
2	After (2) FFT , the frequency domain channel estimate can be used to compensate for multiplicative distortion by using (3) One-tap Equalizer .
3	Using (4) Data Detector , the estimated data is produced.
4	Using the results from step1 and step3, ICI term can be estimated from (5) ICI Generator .
5	The ICI term can be taken away from received signal Y by using (6) Parallel ICI Canceller .
6	If the iteration time $n < N_I$, go to step1.

4.3.3 Complexity Issue

In this section, we discuss the complexity issue in the PIC structure shown in Figure 4-7 which occupies major part of the computation load per iteration. In the first

stage, it requires N one-tap equalizers to compensate for the multiplicative distortion. As seen in Figure 4-1, most of the energy of the time-varying channel is concentrated in the neighborhood of the dc component in the frequency domain, and the ICI term mainly comes from only a few neighboring subcarriers. It implies that, to reduce the complexity, each desired subcarrier requires only $2d$ neighboring subcarriers to generate the ICI estimate:

$$ICI_i = \sum_{d=i-d, d \neq i}^{i+d} \tilde{H}_{i,d} X_d . \quad (4-38)$$

Since the computation for \mathbf{c}_m^0 , \mathbf{c}_m^1 , and $\Xi^{(p)}$ in (4-14) and (4-29) are fixed, for each channel term $\tilde{H}_{i,d}$, both piece-wise linear approach and Taylor approximation approach require only $2L$ multiplications to perform the FFT. Therefore, each desired subcarrier requires $4dL$ multiplications in the second stage.

For the PUSC mode in mobile WiMAX system, the data is transmitted in certain group of subcarriers per frame. We assume the data transmission occupies q subcarriers, and then the total number of multiplications required for the PIC equalizer would be $N + 4qdL$ per iteration.

4.4 Computer Simulations

In this section, computer simulations are conducted to evaluate the performance of the proposed ICI cancellation system. In the following simulations, the multipath number L and delay vector $\boldsymbol{\tau}$ are assumed to be perfectly known to the receiver. The symbol time and the subcarrier spacing are fixed. The CP length is chosen as $T_b/8$ to ensure the maximum delay spread to be smaller than the CP length, and the

modulation scheme used here is 16QAM. Table 4-2 lists all the parameters used in our simulations and gives all the scalability parameters used for the different FFT sizes and bandwidths. SOFDMA is used following IEEE 802.16-2005, which means that symbol time is constant no matter which FFT length is chosen.

Table 4-2: parameters of the simulated system

Parameter	Value			
FFT length	128	512	1024	2048
Bandwidth (MHz)	1.25	5	10	20
Sampling frequency (MHz)	1.43	5.71	11.4	22.8
Carrier frequency (GHz)	2.5			
Useful Symbol Time T_b (μs)	89.6			
Guard Interval (μs)	11.2			
Mode	PUSC			
Modulation	16QAM			
Code rate	1/2			

In the simulation results, BER performance as a function of SNR is evaluated. The SNR is the receive SNR, which is defined as the ratio of the average total signal power received through all the channel paths to the average received noise power. With the consideration of practical implementation, we evaluate the performance under time-varying multipath channel effect using Vehicular A channel model. The

parameters of multi-path fading channel model for Vehicular A channel is shown in Table 4-3. The individual multi-path is subject to the independent Rayleigh fading, whose time domain correlation is implemented by the Jakes model.

Table 4-3: Channel model used in the simulations

Vehicular A environment		
Tap	Relative delay (ns)	Average power (dB)
1	0	0
2	310	-1
3	710	-9
4	1090	-10
5	1730	-15
6	2510	-20

To see that ICI can be totally cancelled if all the estimates are perfectly known, we compare the BER performance between the schemes with and without ICI cancellation in Figure 4-9. Since our ICI cancellation approach uses first and second order derivative terms to represent the ICI, we eliminate the higher order derivative terms of the time-varying channel under 150 km/hr velocity. The scheme without ICI cancellation uses only the one-tap equalizer to compensate for the channel effect based on the time domain LS channel estimate. Severe error floor can be seen in the graph, indicating the necessity for performing the ICI compensation. The result shows that if the channel estimate is perfectly known and the data is perfectly detected, the ICI term can be perfectly canceled and thus good performance can be expected.

In practical systems, the estimation cannot be anticipated to be perfect and we have to see which block in the overall system described in Figure 4-8 is the most critical part for performance improvement. Comparisons of the different blocks are shown in Figure 4-10 and Figure 4-11. In the legend, the expression of A+ICI(B)

denotes the system with channel estimation approach A, ICI cancellation with Taylor series approximation method, and the data detection approach B. From the simulation results, no matter the channel estimate is perfect and the channel only vary with first and second derivate terms or not, the performance is almost the same if the data detection uses only the nearest data detection technique. But if the data detection is perfect, the ICI cancellation scheme apparently achieves good performance. We can conclude that the channel estimation and ICI cancellation techniques are adequate for compensating the ICI effect if the data can be detected reliably. Figure 4-11 shows that for high mobility, Taylor series approximation which only estimates the ICI term with first and second order derivative terms may not be sufficient to generate the ICI information to be cancelled.

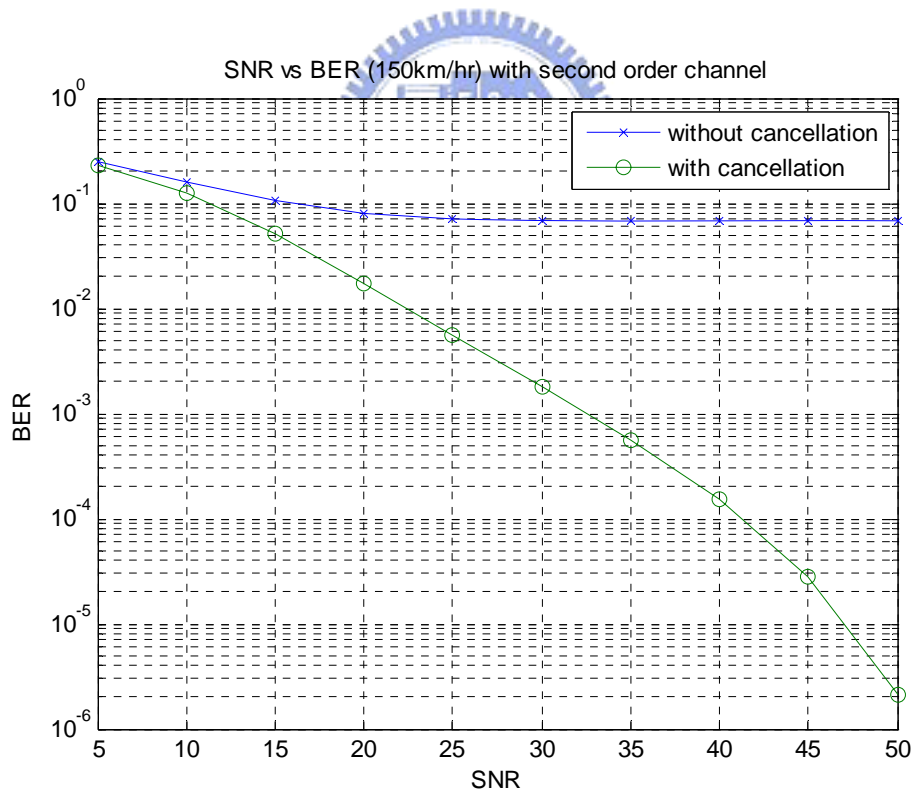


Figure 4-9: Comparison of schemes without and with ICI compensation in second-order varying channel

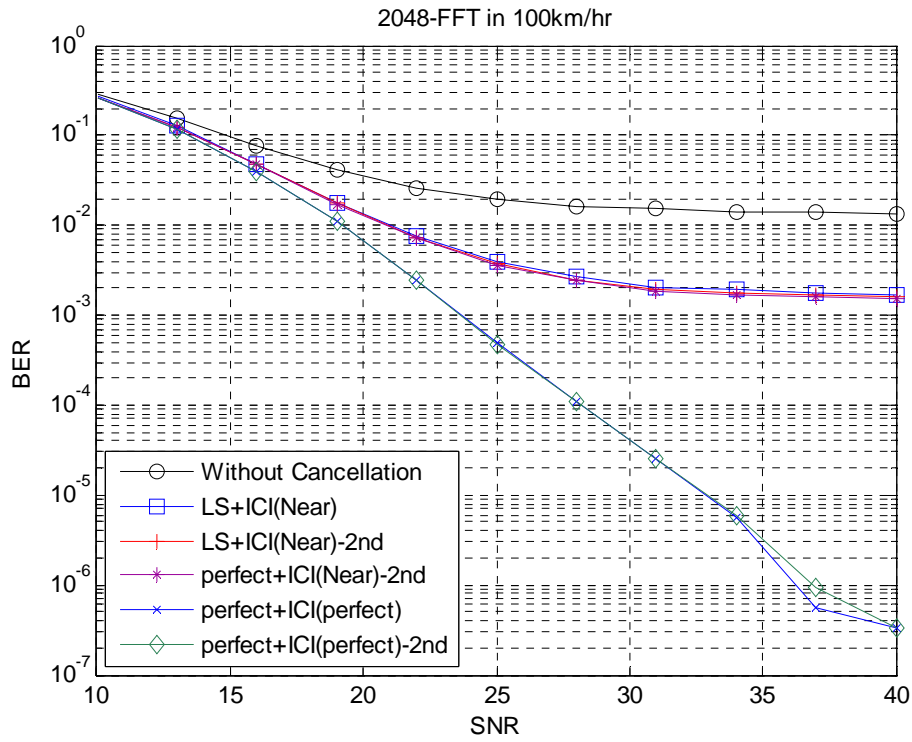


Figure 4-10: Comparison of different blocks with different SNRs

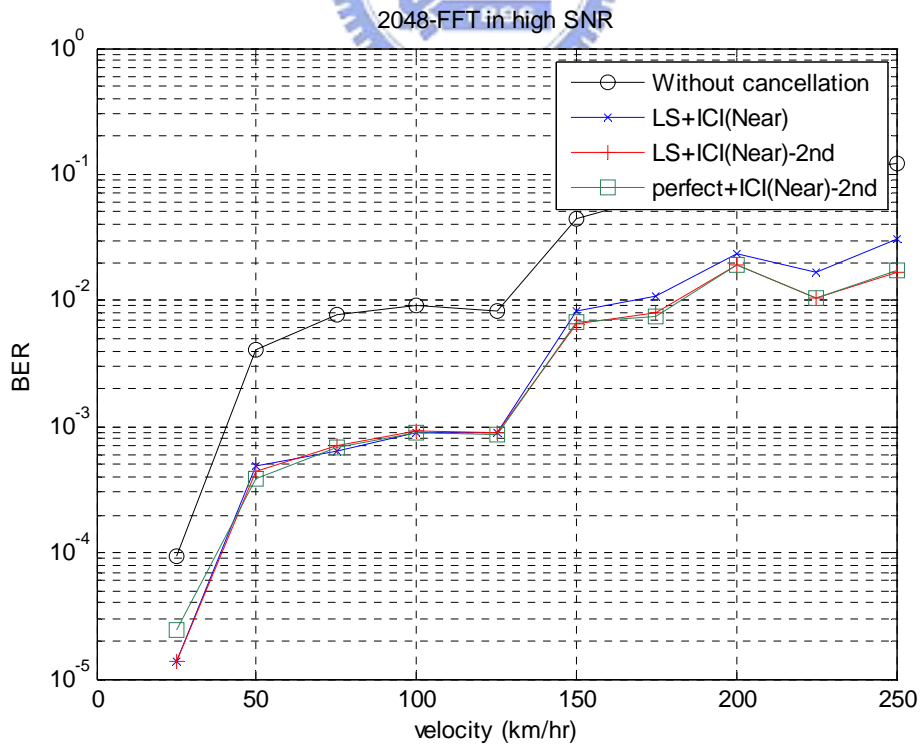


Figure 4-11: Comparison of different blocks under different vehicle speeds

Figure 4-12 shows the BER performance for different d described in 4.3.3. To reduce the complexity, d has to be chosen as small as possible without major performance degradation. From the figure, we can see that there would be no much performance improvement when d is larger than 20. In Figure 4-13, BER performances for different modulation schemes are displayed. Scalability of OFDMA gives the same performance for different FFT size under equal vehicular speed. The support for mobility with transmission using different bandwidths is thus verified.

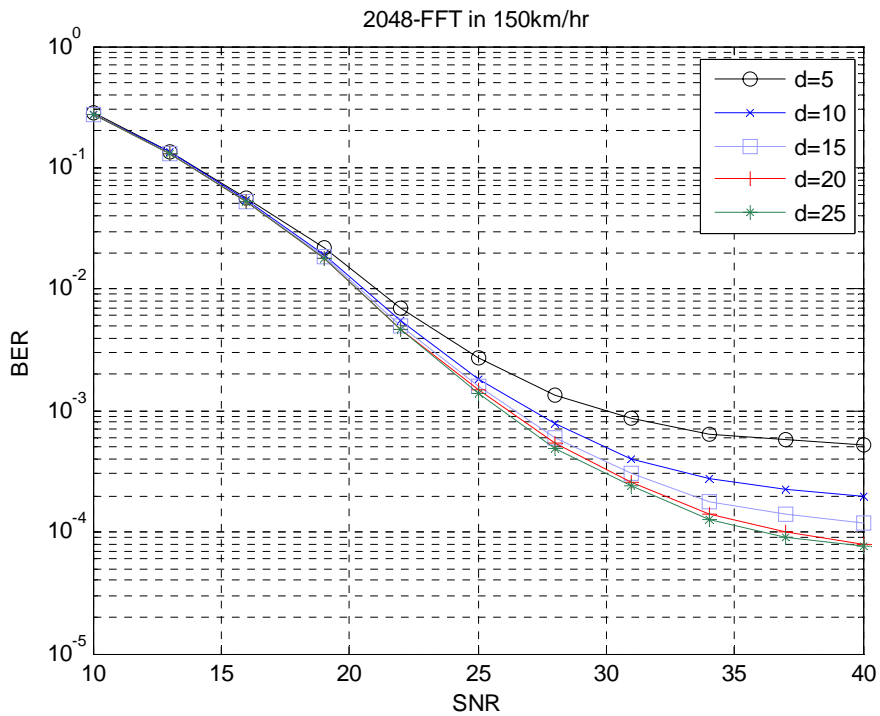


Figure 4-12: BER performance of different d under 150 km/hr

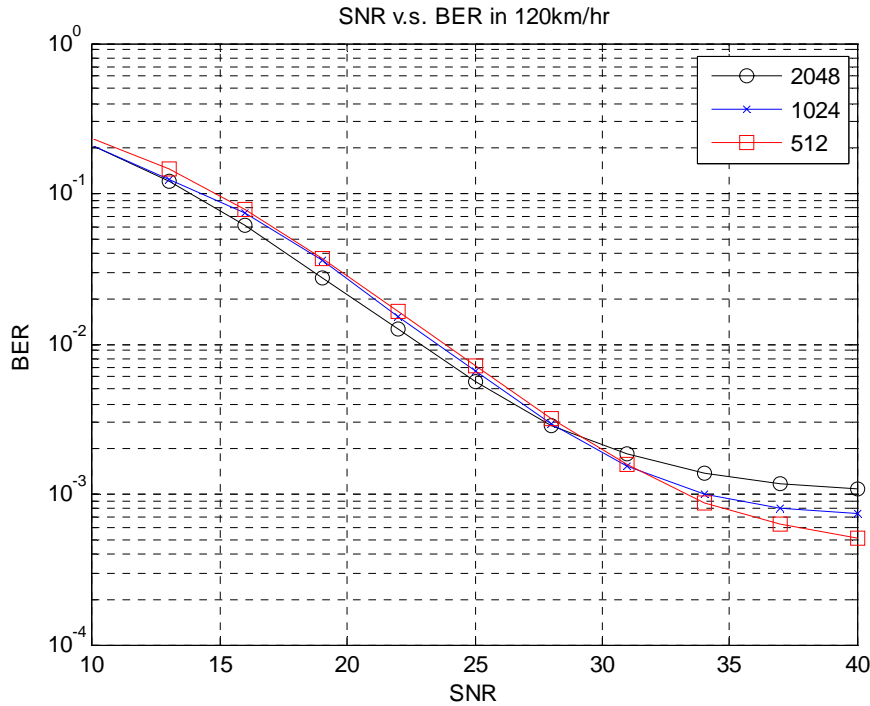


Figure 4-13: BER performance for different modulation schemes under 120 km/hr

At last, BER performances for different SNRs or speeds are shown in Figure 4-14 and Figure 4-15. In the legend, the ICI cancellation techniques used are given in bracket, which are “paper”, “piece-wise”, “Taylor iter1”, and “Taylor iter2”. The “paper” technique used in [9] constructs the channel matrix similar to (4-19) using the piece-wise linear approximation and then detect data using the inverse of the matrix. The disadvantage of this method is the vulnerability against inaccurate estimates in mobile environment. The simulation has shown that the PIC structure described in this thesis can reduce the error floor of the technique used in [9]. We can also observe that the performance improves as the iteration number N_I grows to 2. From Figure 4-15, under high mobility, the difference between the two techniques, piece-wise linear approximate and Taylor series approximation, will increase due to the extra second order derivative terms of the time-varying channel.

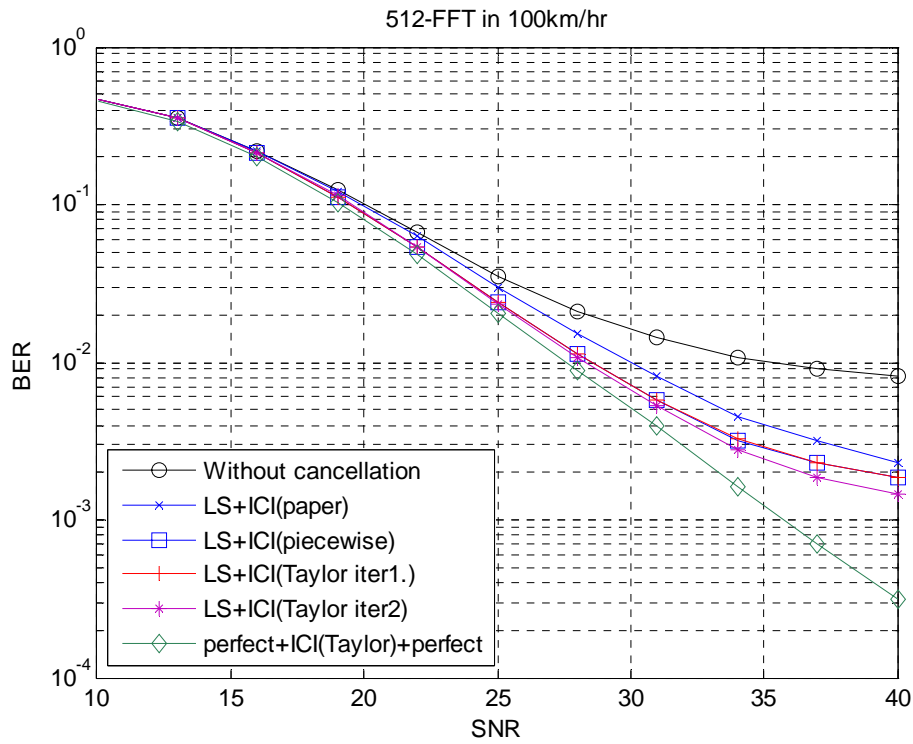


Figure 4-14: BER performance for different methods with 512-FFT under 100 km/hr

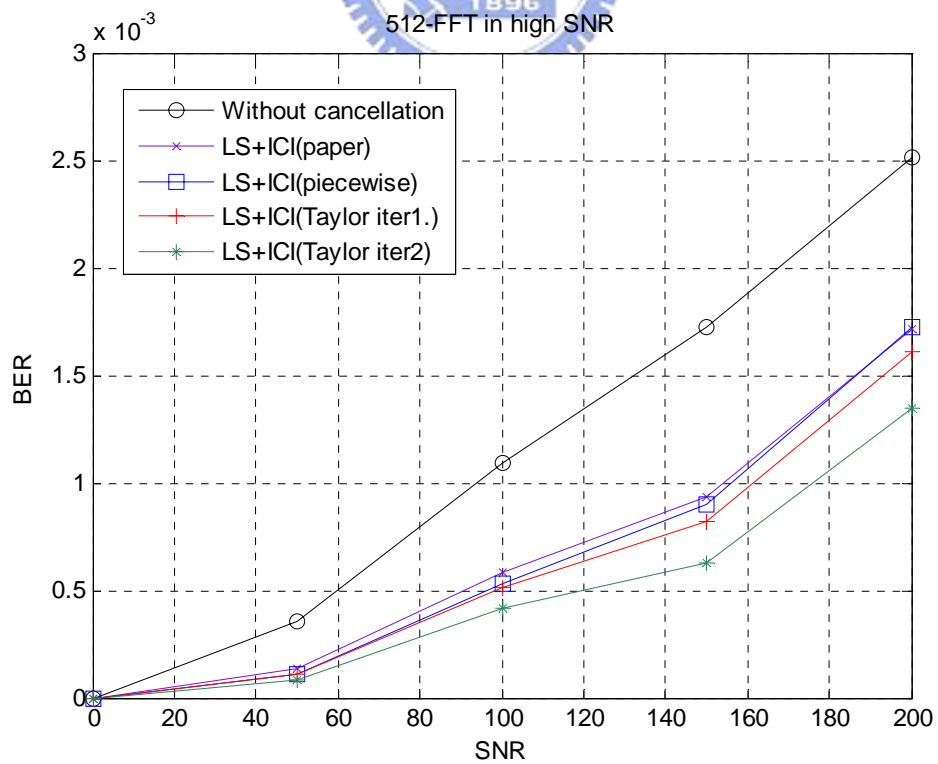


Figure 4-15: BER performance for different methods with 512-FFT under high SNR

4.5 Summary

In this chapter, we first introduce the channel effect in mobile environment. Two methods, piece-wise linear and Taylor series approximation, are used to obtain the ICI information from the channel estimate. Then, the PIC equalizer is introduced and the complexity issue for two stages of the equalizer is discussed. The proposed iterative system structure combined with channel estimation and ICI cancellation is introduced in detail. At last, the computer simulation results show that the proposed scheme using IEEE 802.16-2005 standard can effectively compensate for the mobile channel effect.



Chapter 5

Conclusion

In this thesis, we propose an iterative ICI mitigation and time-varying channel estimation scheme, which can model the ICI using piece-wise linear or Taylor series approximation from the channel estimate and then cancel it using PIC equalizer. Compared with conventional one-tap equalizers, this scheme can achieve better performance in mobile environments. Also, the system is constructed following the OFDMA mode in the IEEE 802.16-2005 standard and is proven to be effective by simulations in mobile environment.

In Chapter 2, the transmitter architecture and specification of IEEE 802.16-2005 system have been introduced. In the rest of this chapter, we also introduce the multiple-antenna transmit techniques such as STC and AAS adopted in the standard. In Chapter 3, we introduce three channel models: the SUI channel model from the fixed wireless channel environment, the ITU channel model for the mobile channel environment, and the SCM channel model for the MIMO mobile channel environment. After that, several channel estimation algorithms and interpolation approaches are introduced. The time domain LS channel estimation has been adopted and the reason why we choose it is also discussed. The estimate obtained from this channel estimator can be further used to compensate the ICI effect in Chapter 4. In Chapter 4, the ICI

induced by the time-varying channel is discussed first. Two approaches of modeling the ICI using the piece-wise linear model and Taylor series expansion with polynomial interpolation are discussed. Afterwards, the PIC equalizer for canceling the ICI is proposed. The entire system structure with channel estimation scheme discussed in Chapter 3, ICI modeling, and PIC equalizer is proposed and can iteratively cancel the ICI effect. In the end, we analyze the complexity of this scheme and simulate the system in mobile environment.

When combating the channel distortion, the conventional system uses only the one-tap equalizer to equalize the channel effect, which would result in large error in mobile environment with ICI produced. Many techniques of compensating the ICI effect have been discussed extensively but may add the computation load significantly and also lacks the entire consideration of the receiver structure. Therefore, the major contribution of this thesis is that the entire system structure is proposed combined with channel estimation and ICI cancellation schemes with moderate complexity and is shown to be useful in practical applications.

Bibliography

- [1] *IEEE Std 802.16e-2005 and IEEE Std 802.16-2004/Cor 1-2005*, “Part 16: air interface for fixed and mobile broadband wireless access systems,” Feb. 2006.
- [2] *IEEE Std 802.16-2004*, “Part 16: air interface for fixed broadband wireless access systems,” Oct. 2004.
- [3] J. A. C. Bingham, “Multicarrier modulation for data transmission: An idea whose time has come,” *IEEE Commun. Mag.*, vol. 28, no. 5, pp. 5-14, May 1990.
- [4] M. Russell and G. Stuber, “Interchannel interference analysis of OFDM in a mobile environment,” in *Proc. Vehicular Technology Conf.-Fall*, 1999, pp. 329-333
- [5] Y. Zhao and S. G. Haggman, “Intercarrier interference self-cancellation schemes for OFDM mobile communication systems,” *IEEE Trans. Commun.*, vol. 49, no. 7, pp. 1185-1191, Jul. 2001
- [6] J. Cai, X. Shen, J. W. Mark, “Robust channel estimation for OFDM wireless communication systems - an H_∞ approach,” *IEEE Trans. Commun.*, vol. 3, no. 6, pp. 2060 – 2071, Nov. 2004.
- [7] S. Tomasin, A. Gorokhov, H. Yang, and J. P. Linnartz, “Iterative interference cancellation and channel estimation for mobile OFDM,” *IEEE Trans. Wireless Commun.*, vol. 4, no. 1, pp. 238-245, Jan. 2005
- [8] W. G. Jeon, K. H. Chan, and Y. S. Cho, “An equalization technique for OFDM

- systems in time-variant multipath channels,” *IEEE Trans. Commun.*, vol. 47, no. 1, pp. 27-32, Jan. 1999.
- [9] Y. Mostofi and D. C. Cox, “ICI Mitigation for Pilot-Aided OFDM Mobile Systems,” *IEEE Trans. Wireless Commun.*, vol. 4, no. 2, Mar. 2005
- [10] W. S. Hou; B. S. Chen, “ICI cancellation for OFDM communication systems in time-varying multipath fading channels,” *IEEE Trans. Wireless Commun.*, vol. 4, no. 5, pp. 2100-2110, Sep. 2005
- [11] “Mobile WiMAX - part 1: a technical overview and performance evaluation,” *WiMAX Forum*, Feb. 2006.
- [12] “Mobile WiMAX - part 2: a comparative analysis,” *WiMAX Forum*, April 2006.
- [13] A. Salvekar, S. Sandhu, Q. Li, M. Vuong and X. Qian, “Multiple-antenna technology in WiMAX systems,” *Intel Technology Journal*, Vol. 8, Aug.2004.
- [14] S. Alamouti, “A simple transmit diversity technique for wireless communications,” *IEEE Journal on Select Areas in Communications*, Vol. 16, No. 8, pp. 1451-1458, Oct. 1998.
- [15] J. J. van de Beek, O. Edfors, M. Sandell, S. K. Wilson, P. O. Borjesson, “On channel estimation in OFDM systems ” in *Proc. 45th IEEE Vehicular Technology Conf.*, Chicago, IL, July 1995, pp. 815-819
- [16] S. V. Vaseghi, *Advanced Signal Processing and Digital Noise Reduction*, Wiley Teubner communications, 1996
- [17] R. Krishnan and T. Kadous, “Channel estimation for OFDM communication systems,” U.S. Patent 7,039,001, May 2, 2006
- [18] *IEEE 802.16a-03/01*, “Channel models for fixed wireless applications,” June 2003.
- [19] *Recommendation ITU-R M.1225*, “Guidelines for evaluation of radio

transmission technologies for IMT-2000,” 1997.

[20] *3GPP TR 25.996*, "Spatial channel model for Multiple Input Multiple Output (MIMO) simulations," v6.1.0, Sep. 2003

[21] M. H. Hsieh and C. H. Wei, "Channel estimation for OFDM systems based on comb-type pilot arrangement in frequency selective fading channels," *IEEE Trans. Consumer Electronics*, Vol. 44, pp. 217-225, Feb. 1998.

[22] Golub and V. Loan, *Matrix Computations*

[23] Lancaster and Timenetsky, *The theory of Matrices*

[24] T. Blu, P. Thevenaz, and M. Unser, "Linear Interpolation Revitalized," *IEEE Trans. Image Processing*, vol. 13, no. 5, pp. 719-719, May 2004.

